AD-A250 981

(2)

'ATION PAGE

Form Approved
OMB No. 0704-0188

1. AGENCY USE ONLY (Leave blank)	2. REPORT DATE	3. REPORT TYPE AND DATES COVERED
	25 February 1992	Final Technical - 15 Aug 90 - 29 Feb 92

4. TITLE AND SUBTITLE
(U) Particle Diagnostics in Optically Thick Sprays

5. FUNDING NUMBERS
PE - 61102F
PR - 2308
SA - CS
G - AFOSR 90-0358

6. AUTHOR(S)
E D Hirleman and S B Kenney

7. PERFORMING ORGANIZATION NAME(S) AND ADDRESS(ES)
Arizona State University
Department of Mechanical and
Aerospace Engineering
Tempe AZ 85287-6106

AFOSR-TR

8. PERFORMING ORGANIZATION REPORT NUMBER
92 0446

9. SPONSORING/MONITORING AGENCY NAME(S) AND ADDRESS(ES)
AFOSR/NA
Building 410
Bolling AFB DC 20332-6448

10. SPONSORING/MONITORING AGENCY REPORT NUMBER

11. SUPPLEMENTARY NOTES

12a. DISTRIBUTION/AVAILABILITY STATEMENT
Approved for public release; distribution is unlimited

12b. DISTRIBUTION CODE

13. ABSTRACT (Maximum 200 words)

The results of a one-year research effort addressing some fundamental scientific issues relevant to particle diagnostics in optically-thick sprays are presented. The objective of this research effort involved development and application of an experimental apparatus for studying scattering in optically thick media. The important technical contributions of this project included 1) development of a fluidized bed approach for creating controlled optically thick media, and 2) characterization of performance of multi-element detectors and light-valve arrays. With respect to the former, we have developed a binary-particle-phase fluidized bed concept combined with refractive-index matching that will allow the bed to be fluid-dynamically very dense (with interparticle spacings on the order of two diameters as required for stable operation) but optically less thick (with interparticle spacings greater than five diameters where independent, as opposed to dependent, multiple scattering is in effect). Conditions for stable operation of the binary-particle-phase fluidized bed have been identified. Regarding detector and light-valve arrays, the experimental results indicated that edge effects are important and that current-generation Faraday-effect light valve arrays do not have the performance specifications required for use in multi-angle interrogation schemes for diagnostics in optically thick sprays.

14. SUBJECT TERMS
Particle Sizing, Droplet Sizing, Sprays, Light Scattering, Multiple Scattering, Optical Diagnostics, Optical Sensors

15. NUMBER OF PAGES
46

16. PRICE CODE

17. SECURITY CLASSIFICATION OF REPORT	18. SECURITY CLASSIFICATION OF THIS PAGE	19. SECURITY CLASSIFICATION OF ABSTRACT	20. LIMITATION OF ABSTRACT
Unclassified	Unclassified	Unclassified	UL

PARTICLE DIAGNOSTICS IN OPTICALLY THICK SPRAYS

Final Report

for

AFOSR Grant 90-0358

for the period

15 September 1990 - 31 December 1991

submitted by

E. Dan Hirleman
Mechanical and Aerospace Engineering Department
Arizona State University
Tempe, AZ 85287-6106
Tele: (602) 965-3895
FAX: (602) 965-1384

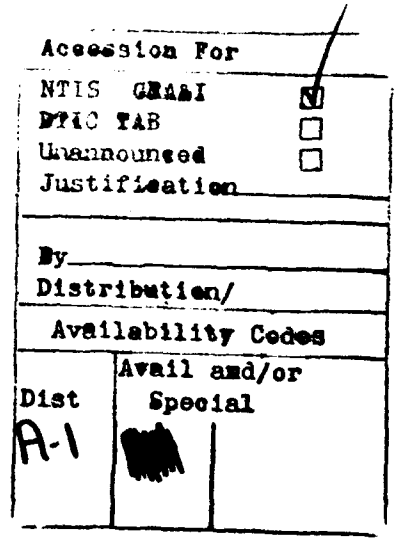

ABSTRACT

The results of a one-year research effort addressing some fundamental scientific issues relevant to particle diagnostics in optically-thick sprays are presented. The objective of this research effort involved development and application of an experimental apparatus for studying scattering in optically thick media. The important technical contributions of this project included 1) development of a fluidized bed approach for creating controlled optically thick media, and 2) characterization of performance of multi-element detectors and light-valve arrays. With respect to the former, we have developed a binary-particle-phase fluidized bed concept combined with refractive-index matching that will allow the bed to be fluid-dynamically very dense (with interparticle spacings on the order of two diameters as required for stable operation) but optically less thick (with interparticle spacings greater than five diameters where independent, as opposed to dependent, multiple scattering is in effect). Conditions for stable operation of the binary-particle-phase fluidized bed have been identified. Regarding detector and light-valve arrays, the experimental results indicated that edge effects are important and that current-generation Faraday-effect light valve arrays do not have the performance specifications required for use in multi-angle interrogation schemes for diagnostics in optically thick sprays.

I. INTRODUCTION

Particle and droplet size distributions, being parameters of fundamental importance, should be priority measurement objectives for intelligent sensors in next-generation propulsion systems. However, the potential application of laser scattering systems as optical sensors introduces some severe requirements on the measurement techniques. In particular, the presence of multiple scattering in the near-field regions of sprays significantly complicate the application of optical diagnostics. This research project involved experimental work related to measurements under such conditions. In particular, a fluidized bed system with the potential for providing a stable medium with controlled and continuously variable optical depth for a constant size-distribution was proposed and studied. The present work was predicated on a preceding project as discussed by Hirleman [1,2].

The long-term objective of this research is to understand the process of multiple scattering as it might occur in future applications of intelligent particle size distribution sensors and develop inversion schemes which can operate in such an environment. A minimum requirement is that the presence of multiple scattering be diagnosed by the instrument to ensure that erroneous data not be used in control algorithms, a situation which could result in a catastrophic failure. Our goal was to surpass that and develop efficient and robust algorithms which can actually extract useful particle size information from Fraunhofer diffraction measurements in multiple scattering environments.

The laser diffraction particle sizing technique comprising the framework for this research has been described in detail in the literature; for current references see [3]. In the sections below, the results of this project are discussed. This final report is intended as an overview and synthesis of the research results as opposed to an exhaustive restatement of what has appeared in previous progress reports, annual reports, and published technical papers. Publications resulting from this work are incorporated by way of references from the technical section. Finally, a summary of personnel involved in the project is presented.

II. FLUIDIZED BED SYSTEM

The creation of a stable and well-characterized two-phase system such as a liquid droplet spray (in a gas) or a dispersion of solid or liquid particles in a liquid is very difficult and has escaped all efforts of standardization. Probably the most straightforward approach to obtain a known calibration particle system for optical instruments is to disperse glass or polystyrene

calibration microspheres available as certified reference materials in a liquid using stirred- or flow-cells. Our early efforts in experimental verification utilized such an apparatus but questions concerning uniform (spatial) dispersion, centrifugal separation (by size) of the particles in broad size distributions, and the performance of the system at very high particle loadings (i.e. at or near the dependent scattering limit) remained in question.

To solve some of the problems associated with cells such as segregation and deposition we designed and constructed a fluidized bed system [4] as shown schematically in Fig. 1 and in a photograph in Fig. 2. In theory, a fluidized bed should provide a uniform dispersion of the particles and therefore a very simple means by which to control the particle concentration and, in turn, the optical depth. The fluidized bed consists of the particles of interest placed in the test section between two microsieves. A fluidizing liquid is pumped in a closed loop around the system which includes a filter. When the fluid passes through the bed the resulting drag force on the particles will, if the velocity is higher than some critical value, overcome gravity and lift the particles. If the system is operating properly, for a given fluid velocity the bed of solid particles will expand until the overall buoyancy and drag forces are balanced. The bed should expand and contract as the flow rate is varied, and the concentration (#/cc) of particles will just depend on the height of the expanded bed and the total number of particles originally placed in the fluidizing section.

The fluidizing section in the bed developed here and shown in Figs. 1 and 2 is 7.62 x 2.54 cm (3 x 1 inch) inner dimensions with a height of 30.48 cm (12 inch). Optical access is provided by two anti-reflection-coated quartz windows providing a 2.54 cm (1 inch) diameter clearance near the bottom of the bed and a 7.62 cm (3 inch) path length for the laser beam. (The capacity for similar windows on opposite sides of the shorter dimension is available). A plexiglass window running the full height of the fluidizing section provides optical access to allow measurement of the bed height for the independent determination of particle concentration. With the two optical paths the system can theoretically allow a 10:1 variation in optical depth *while maintaining the same particle size distribution* by merely adjusting the flow rate. The absolute values of the optical depths are determined by the number (mass) of particles placed in the fluidizing section of the bed when it is assembled.

We have successfully stabilized the operation of the fluidized bed under several conditions. A photograph of the system in operation is given in Fig. 3. However, the stable operating conditions we have found have been for void fractions (defined as liquid volume divided by the total volume of the bed) too low for the multiple scattering models relevant here. In particular, 90% void fraction is the highest value for which we have achieved stable operation. At higher values of void fraction, the bed underwent the well-known "spouting" phenomenon and the necessary uniform spatial distribution of the particle phase was lost. This level of void fraction (90%) corresponds to an interparticle spacing of approximately 2.7 diameters, a value which falls within the *dependent scattering* regime of Fig. 4. While dependent scattering is of general interest, the objective of this project, based on multiple scattering models developed in the previous work that apply only in the *independent scattering* regime, therefore requires higher void fractions.

To overcome the problem of insufficient void fraction, we propose a binary-particle-phase fluidized bed. This idea is original, and no reference to a similar concept has been found to date. The solid phase of the bed will be comprised of two discrete modes, one which we designate as the fluidizing particle medium and the other as the scattering medium. These are differentiated via the use of a refractive-index-matching fluid which renders the fluidizing particle medium invisible. The scattering particles are of a different refractive index and are therefore visible and scatter light passing through the bed. The scattering phase must have the same fluid dynamic properties as the fluidizing particle phase so as to not be segregated by the

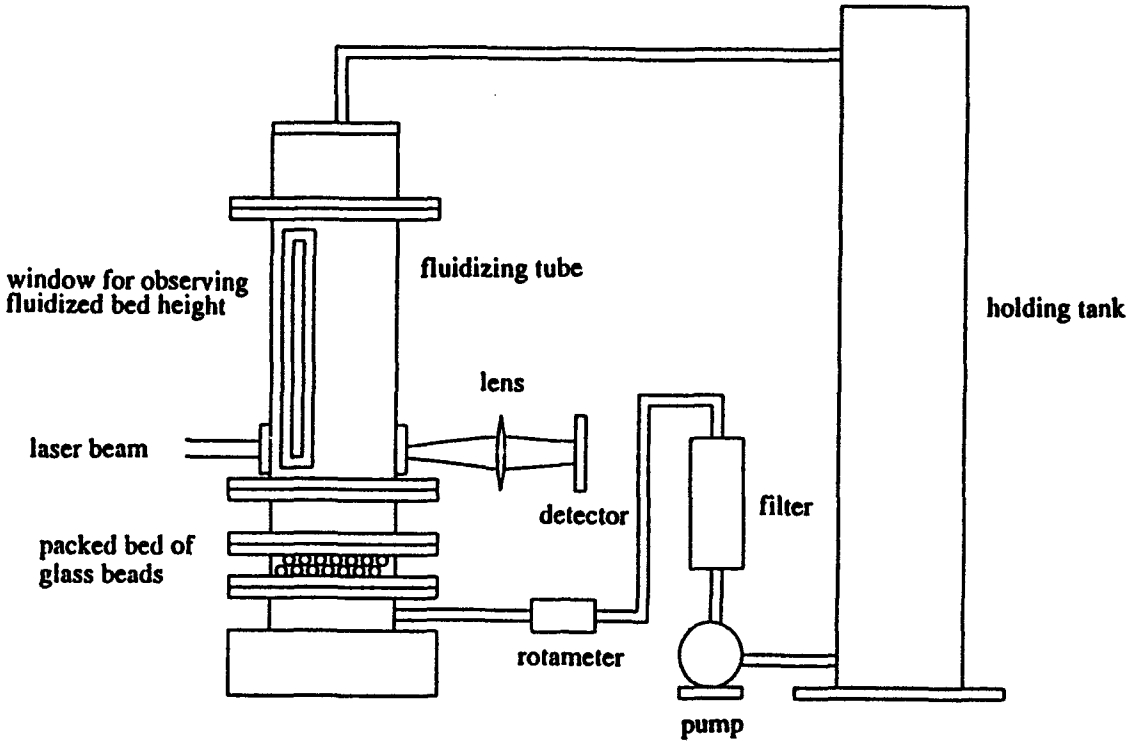

Figure 1. Schematic of the ASU fluidized bed system.

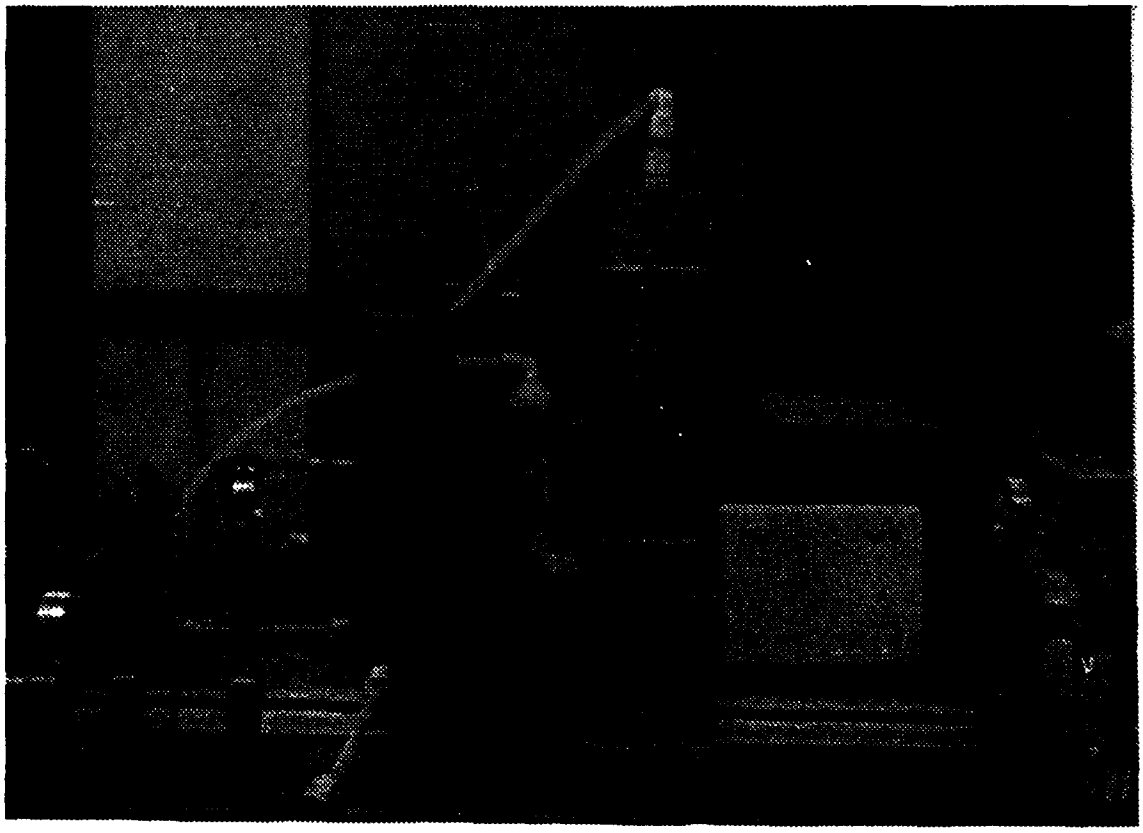

Figure 2. Photograph of the ASU fluidized bed system.

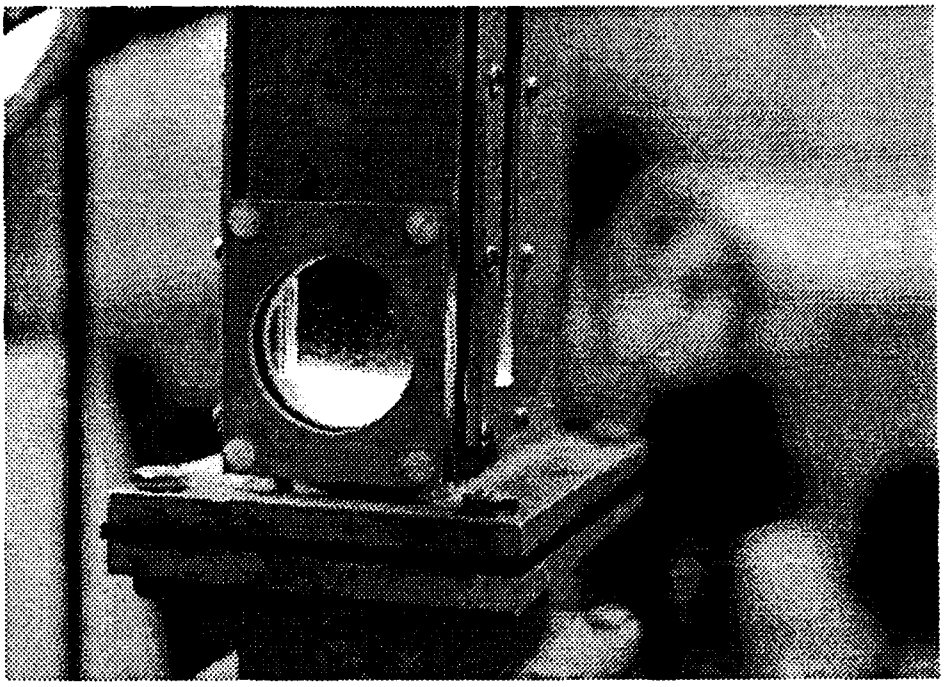

Figure 3. Photograph of the test-section of the ASU fluidized bed system in operation. The fluid was water, and the particle phase was made up of glass beads in the 74 - 105 μm diameter range obtained from Cataphote Corp. The operation was stable at this condition, with a bed height of 3.8 cm (1.5 inch).

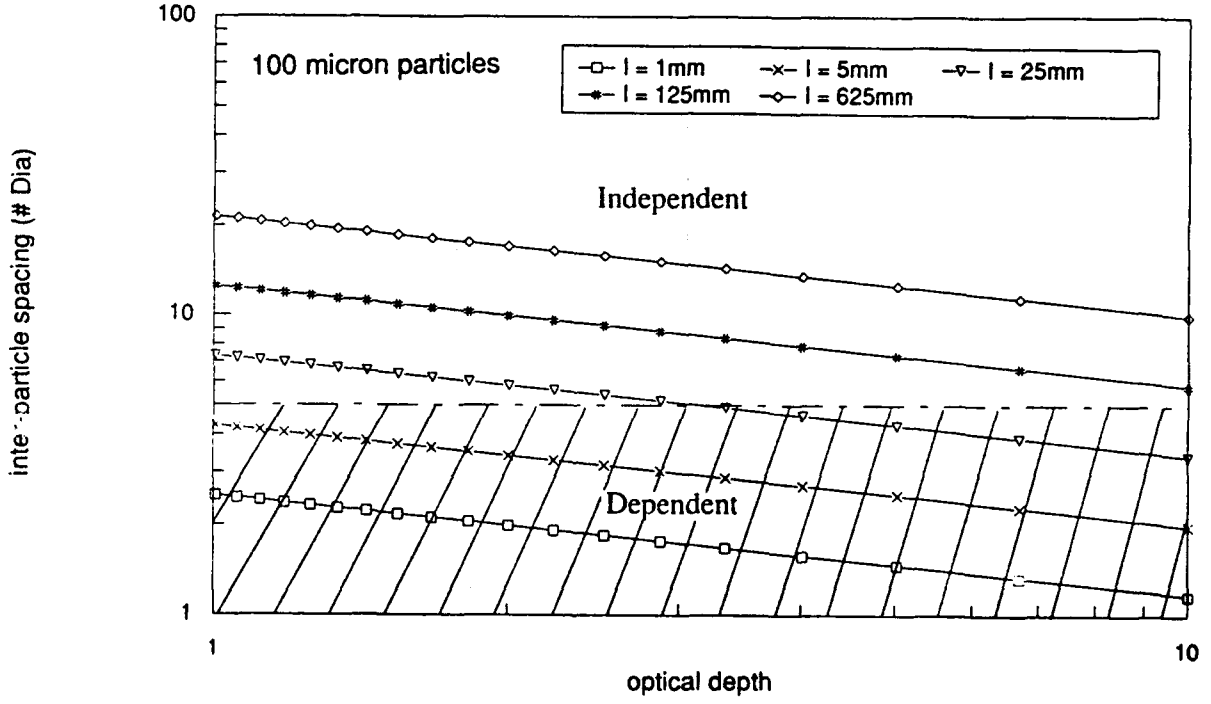

Figure 4. Optical property map for a fluidized bed. Curves of constant physical path length l are shown vs. inter-particle spacing and optical depth for 100 μm spheres. The regimes of dependent and independent scattering are shown as well.

fluidized bed. In this way the void fractions of the two solid particle phases are independently variable, thereby allowing control of the optical depth of the medium independent of the total void fraction. In this way the bed can be operated in a fluid-dynamically stable regime while optically in the independent scattering regime as is required for this work.

The design problem basically then involves selection of the properties of the two particle phases and the fluid. One critical constraint is that the fluidizing particle phase must be optically homogeneous, i.e. no inclusions or other inhomogeneities inside the particles can be tolerated. We have had difficulty obtaining particles of acceptable quality. In order to achieve refractive-index matching, it is easier to obtain fluids to match the refractive index of a given particle rather than vice-versa. To check for a refractive index match we developed a procedure based on the Beck's Line method that uses refraction phenomena near the edge of a particle to qualitatively ascertain the ratio of the refractive indices of the particles and the fluid. Figures 5 and 6 show photographs taken through a microscope (40X objective) of glass beads in the 74-105 μm diameter range obtained from Cataphote Corporation immersed in Cargille fluids of refractive index 1.51 and 1.52 respectively. In Fig. 5, the outline of the particles are quite visible indicating that the specified nominal refractive index of the particles of 1.51 is off. Also clearly visible in Fig. 5 are a number of impurities and inclusions within the spherical particles that remain visible. These inclusions would scatter light in an experiment and therefore render these particles unacceptable for the binary-particle-phase bed. Figure 6 is a similar photograph where the particles have been immersed in a fluid of refractive index 1.52 where excellent matching has occurred. The outlines of the particles are effectively invisible, though the inclusions within the particle remain visible.

Due to the rather poor optical quality of these particles shown in Figs. 5 and 6, it was necessary to look elsewhere for particles. Some example of spheres of better quality are shown in Figs 7 and 8. Probably the best quality particles we have tested are the high-index spheres from Duke Scientific Corp. shown in Fig. 8. The problem with these is the high refractive index of 1.91, since the available refractive index fluids in that range are highly toxic (Arsenic compounds) and certainly very difficult to use. Pyrex particles obtained from Mo-sci near the end of the project have reasonably good quality and are shown in Fig. 9.

Our proposed design of the binary-particle-phase fluidized bed would involve Mo-sci Pyrex or Yttrium-Alumina-Silica beads as the fluidizing particle medium matched with Cargille fluids and the high density glass microspheres from Duke Scientific as the scattering medium. For stable operation in the ASU fluidized bed for optical depths of 1 - 10 we propose 600 μm diameter particles for the fluidizing particle and 420 μm diameter for the scattering medium.

As of the conclusion of this project we have been unable to demonstrate the binary-particle-phase fluidized bed concept. The particles and fluids required for our proposed design are estimated (based on retail pricing at small quantity prices) of the order of $10,000. Demonstration of our binary-particle-phase fluidized bed concept will be the subject of future work.

III. CHARACTERIZATION OF DETECTOR AND LIGHT VALVE ARRAYS

In the previous project [1] we suggested a possible scheme for a general solution to Fraunhofer diffraction particle size measurements in multiple scattering environments. The experimental system to allow multi-angle interrogation of the particle field is shown in Fig. 10. The key difference between Fig. 10 and conventional single scattering Fraunhofer instruments is the presence of a programmable mask in the front focal plane of the transmitter lens. The programmable mask has annular ring apertures which can be individually switched on (transmitting) or off (absorbing or opaque). A ring of light in the front focal plane of an ideal

Figure 5. Photograph of particles in matching fluid taken through an optical microscope with a 40X objective and a red filter. The particles (of diameter nominally one-third of the field-of-view) are glass beads in the diameter range 74-105 μm obtained from Cataphote Corp. The glass beads have a specified nominal refractive index of 1.51, and they are dispersed in a matching fluid of refractive index 1.51 obtained from Cargille.

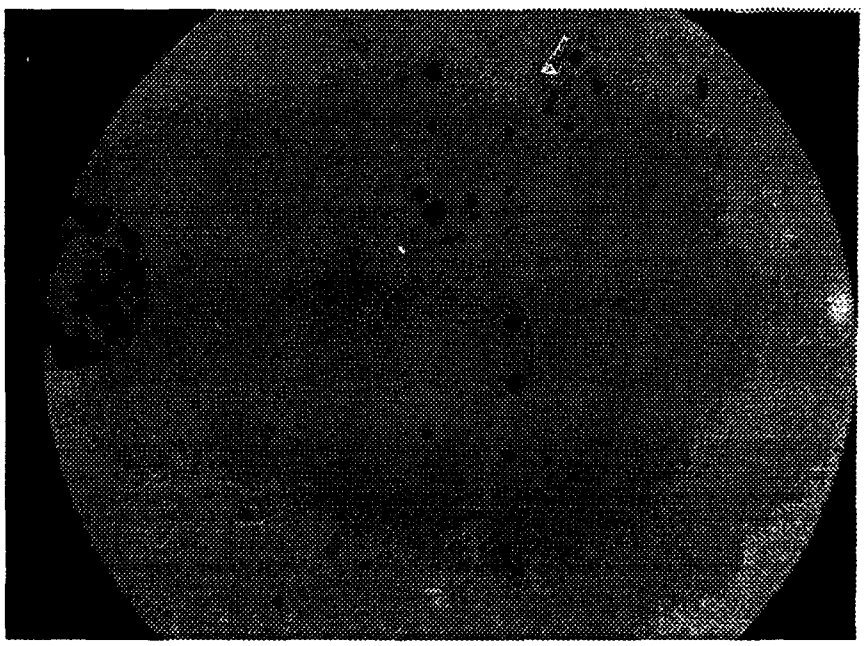

Figure 6. Photograph of particles in matching fluid taken through an optical microscope with a 40X objective and a red filter. The particles (of diameter nominally one-third of the field-of-view) are glass beads in the diameter range 74-105 μm obtained from Cataphote Corp. The glass beads have a specified nominal refractive index of 1.51, and they are dispersed in a matching fluid of refractive index 1.52 obtained from Cargille. The refractive index matching here is quite good, and basically only the inhomogeneities inside the particles are visible.

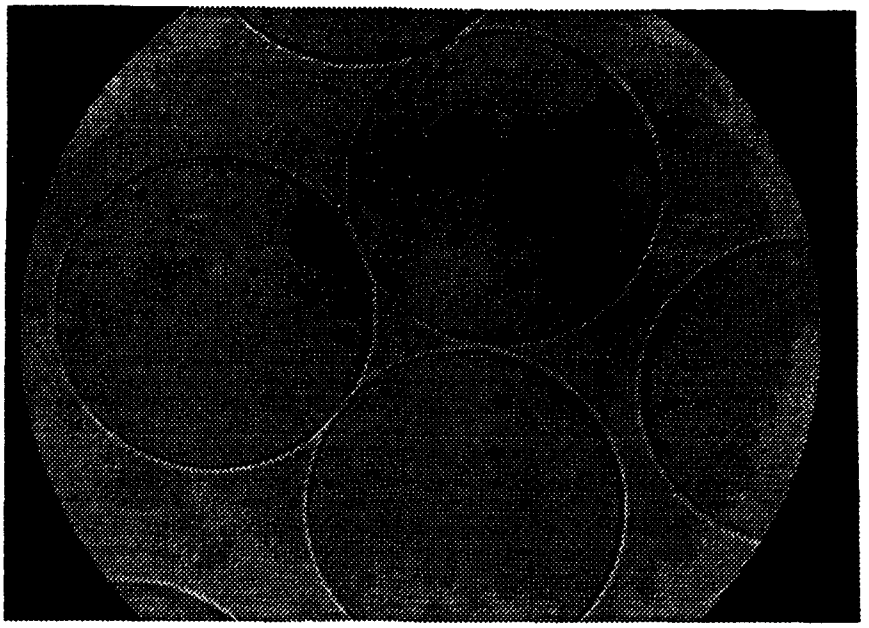

Figure 7. Photograph of particles in matching fluid taken through an optical microscope with a 40X objective and a red filter. The particles (of diameter nominally one-half of the field-of-view) are Yttrium-Alumina-Silica beads of nominally 100 μm diameter obtained from Mo-sci Co. The YAS beads have a specified nominal refractive index of 1.69, and are dispersed in a matching fluid of refractive index 1.69 obtained from Cargille.

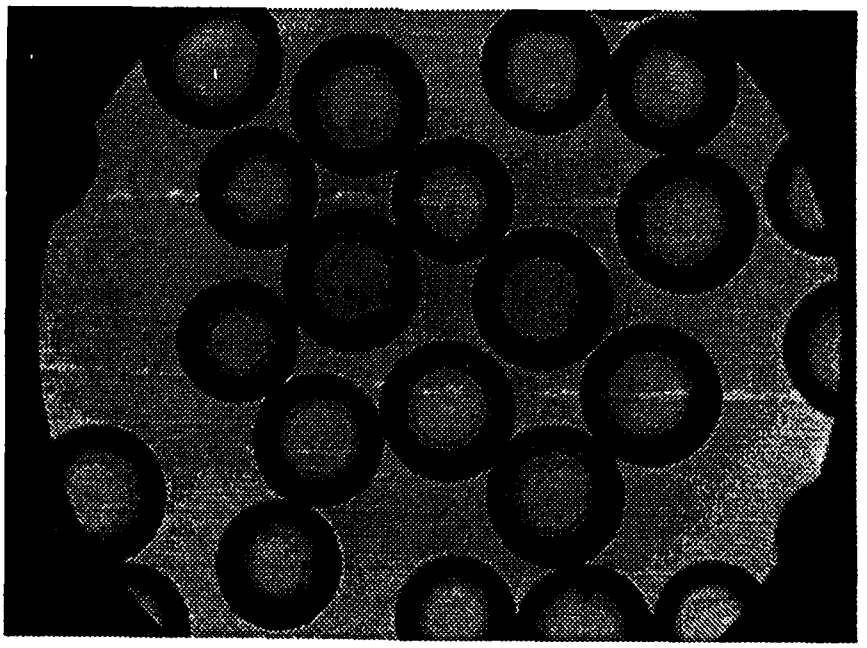

Figure 8. Photograph of particles in matching fluid taken through an optical microscope with a 40X objective and a red filter. The particles (of diameter nominally one-sixth of the field-of-view) are high density glass microspheres obtained from Duke Scientific. The glass microspheres have a specified nominal refractive index of 1.91, and are dispersed in a fluid of refractive index 1.54 obtained from Cargille.

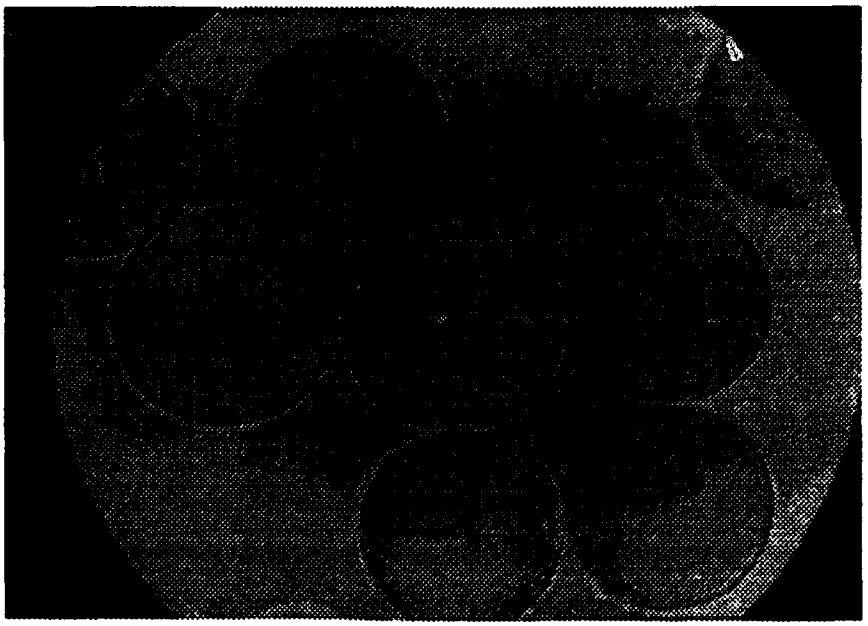

Figure 9. Photograph of particles in matching fluid taken through an optical microscope with a 40X objective and a red filter. The particles (of diameter nominally one-fourth of the field-of-view) are Pyrex spheres obtained from Mo-sci Co. The spheres have a specified nominal refractive index of 1.49, and are dispersed in a fluid of refractive index 1.54 obtained from Cargille.

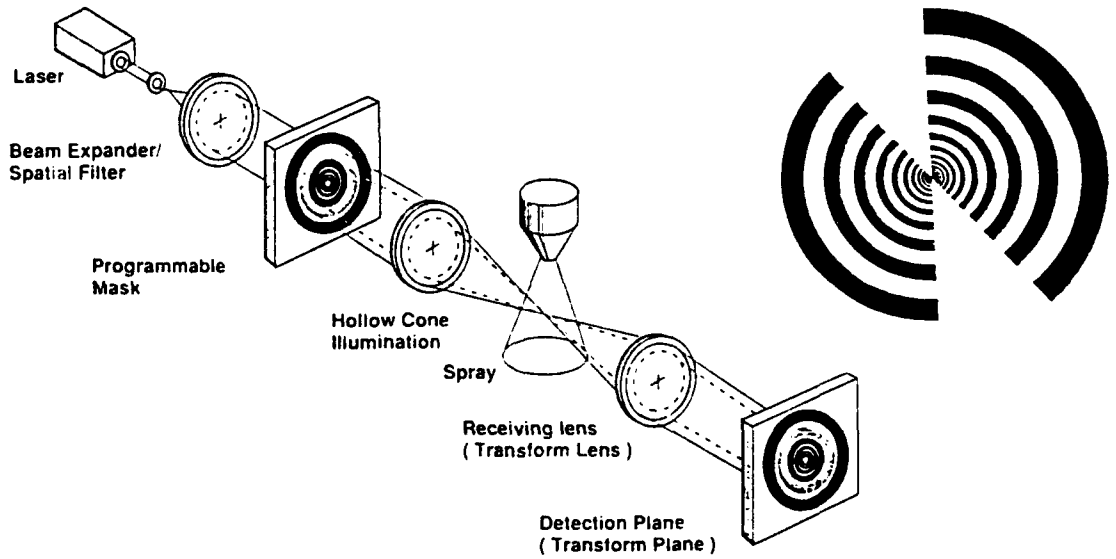

Figure 10. Schematic of optical system for multi-angle interrogation of optically thick sprays. The programmable mask on the input side transmits cylindrical shells of light which are converted to hollow cones of light by a lens. A matched programmable mask at the transform plane allows measurement of the redistribution matrix. The insert shows the actual geometry of the 34-element ring-aperture light valve designed and fabricated according to the optimal scaling law developed by Hirleman [5] in the preceding project.

transmitter lens produces a hollow cone of light of constant angle θ passing through the spray or particle sample volume. By switching open the various rings, a sequence of hollow cones of probe radiation is created. The fraction of the incident energy in the cones which is not scattered by the medium is redirected by the transform lens to a ring on the detection plane which matches the ring in the programmable mask (assuming the focal lengths of the transmitting lens and the transform lens are equal). Light which is scattered by particles in the spray leaves at some angle different than the cone angle and ends up at another radial position (i.e. a different detector ring) on the detector plane.

The method proposed for generating the cones of light necessary for implementing the multi-angle interrogation scheme proposed by Hirleman [2] for deconvolution of the multiple scattering effect involves the use of Faraday-effect light-valve-arrays. Three custom devices have been fabricated based on the optimal scaling geometry of Hirleman [5]. Initial efforts at experimental verification are reported by Kenney and Hirleman [4]. The success of the method hinges on the performance of detector and light valve arrays. The contrast ratio must be such that there is minimum cross-talk between elements. Our efforts at utilizing these devices have basically been unsuccessful. The problem appears to involve the performance of the individual elements. It was necessary to perform a careful characterization of the performance of these devices in order to isolate and quantify the problem.

The experiments used in the portion of the work were similar to those reported by Kenney and Hirleman [6,7,8]. A laser beam was focussed onto the light valve array and a photodetector was placed in line with the beam behind the light valve to collect the transmitted light. The results from a scan across two detector elements of the light-valve array are shown in Fig. 11 for the light valves electronically switched on (open) and then off (closed). The contrast ratio observed for this experiment is about 6, significantly less than that observed in work supported during the previous project by Hirleman and Dellenback [9]. It appears that the performance of the devices has degraded over the past year, and is now at a stage where the cones of light generated by the device are not adequate for the application. Significant advances in the technology will be required before Faraday-effect devices will be usable in the multi-angle interrogation scheme proposed here.

Results of some additional characterization experiments on the arrays are shown in Fig. 12. Here the focussed laser beam (nominally 30 μm diameter) was scanned across the entire array by moving the array in 2.5 μm steps. Also shown in the lowest Fig. 12 are similar results indicating the resolution of the experiment obtained by scanning beam across a knife edge. It is seen that the edge definition on the light valve array is considerably better than that for photodiode array as reported by Kenney and Hirleman [7,8]. The uniformity across the element, as indicated by the fluctuations in transmitted energy at the tops of the waveforms in Figs. 11 and 12 is similar to that we measured for photodiode arrays [7,8].

In summary, the performance of the light valve arrays fabricated for this project was not adequate for incorporation into multi-angle interrogation schemes for diagnostics in optically thick sprays. At present, until technology advances improve the performance of the light valves significantly, other means must be used to generate the interrogation beams. Future work will use axicons or reflexicons to this end

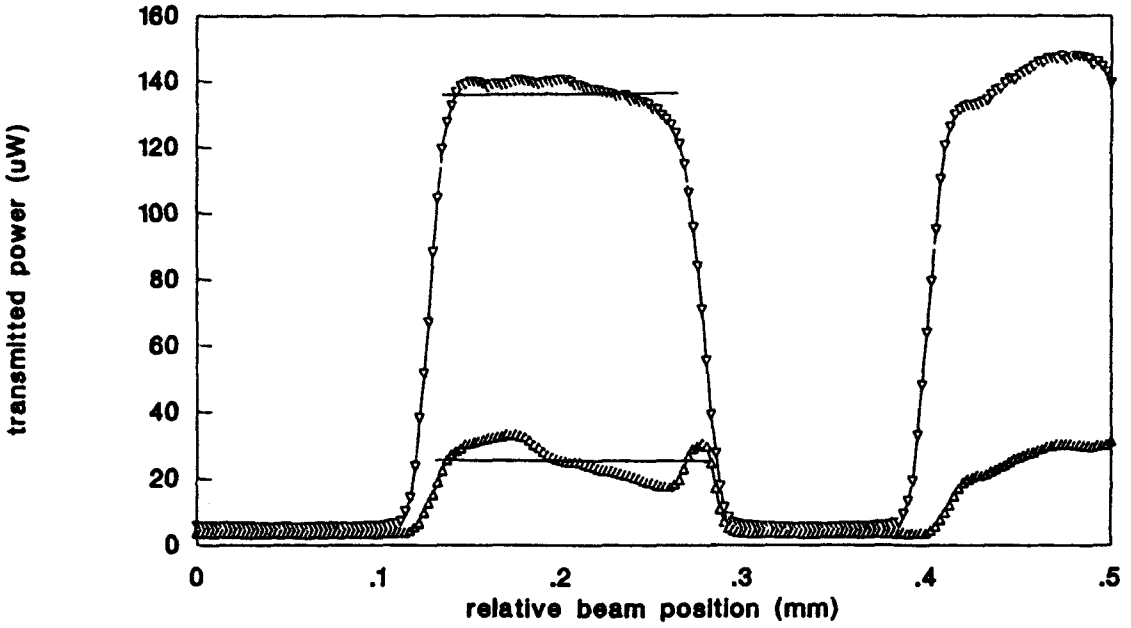

Figure 11. Plot of light transmitted through the ASU light valve array for *on* (∇) and *off* (Δ) cases. The measured contrast ratio for the two ring elements shown is about 6. The data were taken with 2.5 μm steps and averaged results from two scans are plotted.

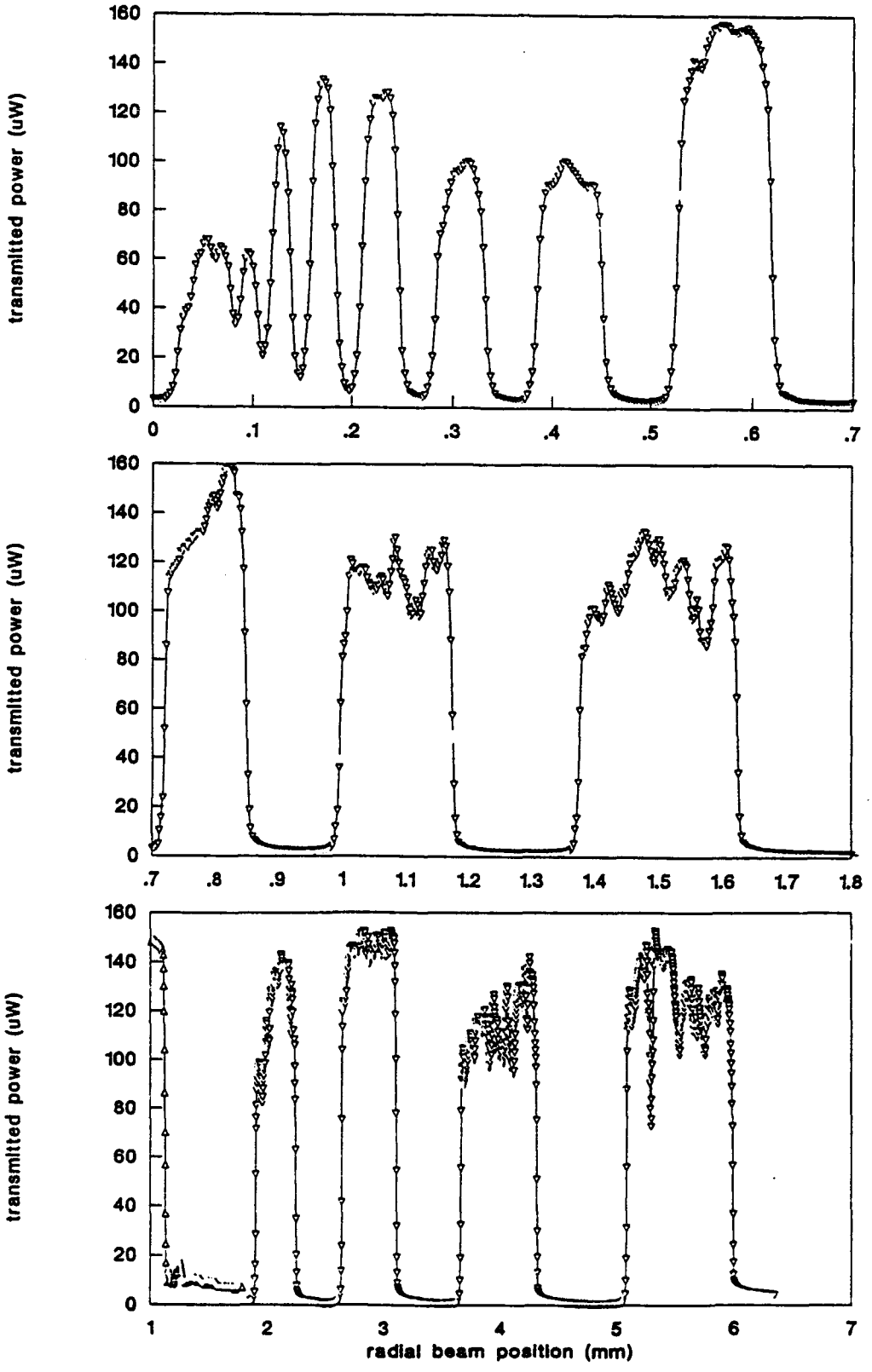

Figure 12. Transmitted optical energy vs. position as a focussed HeNe laser beam was scanned across the ASU light valve array from the center. A knife-edge scan of the beam (see data indicated by Δ on the left side of the lower figure) indicated a beam diameter ($1/e^2$ intensity points) of 30 μm . The edge definition of the light valves edges is much better than 30 μm. The transmission indicated through the inner rings (upper figure) does not saturate since the rings are thinner than the laser beam.

IV. PUBLICATIONS (AND REFERENCES FOR PRECEDING SECTIONS)

1. E. D. Hirleman, "Research on Certain Aspects of Laser Diffraction Particle Size Analysis Relevant to Autonomous, Self-diagnosing Operation." Final Report for AFOSR Project 84-0187, July 27, 1990, Air Force Office of Scientific Research, Bolling Air Force Base, DC.

2. E.D. Hirleman, "A General Solution to the Inverse Near-Forward Scattering Particle Sizing Problem in Multiple Scattering Environments: Theory", *Applied Optics*, V. 30, pp. 4832-4838, 1991.

3. E. D. Hirleman and C. F. Bohren, "Optical Particle Sizing: an Introduction by the Feature Editors", *Applied Optics*, V. 30, pp. 4685-4687, 1991.

4. S. B. Kenney and E. D. Hirleman, "A General Solution to the Inverse Near-Forward Scattering Particle Sizing Problem in Multiple Scattering Environments: Experiments", pp. 27-30 in *Proceedings of the 2nd International Congress on Optical Particle Sizing, Post-Deadline Papers Addendum*, Arizona State University, Tempe, AZ, 1990.

5. E. D. Hirleman, "Optimal Scaling for Fraunhofer Diffraction Particle Sizing Instruments," *Particle Characterization*, Vol 4, pp. 128-133, 1988.

6. S. Kenney, "Particle Size Analysis Using Integral Transform Techniques on Fraunhofer Diffraction Patterns," M.S. Thesis, Mechanical and Aerospace Engineering Department, Arizona State University, May, 1991.

7. S. B. Kenney and E. D. Hirleman, "Edge Effects in Silicon Photodiode Arrays", pp. 82-93 in *Sensors and Sensor Integration*, Peter Dean, Editor, Proc. SPIE 1480, SPIE, Bellingham, WA, 1991.

8. S. B. Kenney and E. D. Hirleman, "Calibration Factors for Laser Diffraction Ring Detectors: Theoretical Modeling", pp. 415-422, *Proceedings of the Fifth International Conference on Liquid Atomization and Spray Systems (ICLASS - 91)*, National Institute of Standards and Technology (NIST) Special Publication 813, U. S. Government Printing Office, Washington D. C., 1991.

9. E. D. Hirleman and P. A. Dellenback, "Adaptive Fraunhofer Diffraction Particle Sizing Instrument using a Spatial Light Modulator", *Applied Optics*, Vol. 28, pp. 4870-4878, 1989.

10. E. D. Hirleman, P. G. Felton, and J. Kennedy, "Results of the ASTM Interlaboratory Study on Calibration Verification of Laser Diffraction Particle Sizing Instruments using Photomask Reticles", pp. 611-620, *Proceedings of the Fifth International Conference on Liquid Atomization and Spray Systems (ICLASS - 91)*, National Institute of Standards and Technology (NIST) Special Publication 813, U. S. Government Printing Office, Washington D. C., 1991.

V. PROFESSIONAL PERSONNEL

Anthony M. Bruner - Undergraduate Lab Assistant and B.S. student. Has assisted the graduate students in the work, particularly regarding software and instrumentation development. He will receive the B.S. in Aerospace Engineering in 1992 and will hopefully attend graduate school.

E. Dan Hirleman - Professor of Mechanical and Aerospace Engineering. Principal Investigator.

Steven B. Kenney - Graduate Research Assistant and M.S. student. Using this project for his M.S. research, Steve received the M.S. degree in Spring, 1991, and his thesis is listed as Ref. [7]. He is presently employed by Morton-Thiokol in Utah.

VI. INTERACTIONS

1. E. D. Hirleman, "Phase-Doppler Particle Analyzer: Performance Characterization and Measurements in Sprays", seminar presented at Technion - Israeli Institute of Technology, Aerospace Engineering Department, July, 1990.

2. E. D. Hirleman, "Calibration Verification of Laser Diffraction Particle Sizing Instruments using Photomask Reticles", Invited Lecture, Panel on Pending Standards and their Impact on the Fine Particle Industry", Fine Particle Society Annual Meeting, San Diego, CA, August, 1990.

3. E. D. Hirleman, "On the Inverse Fraunhofer Diffraction Particle Sizing Problem", Mechanical Engineering Department Seminar, Purdue University, W. Lafayette, IN, October, 1990.

The following lectures were presented as a Distinguished Lecturer Colloquia Series in the Mechanical Engineering Department, University of Minnesota, Minneapolis, MN.

4. E. D. Hirleman, "Particle Diagnostics using Optical Techniques: Introduction", Mechanical Engineering Department, University of Minnesota, Minneapolis, MN, May, 1991.

5. E. D. Hirleman, "Ensemble Particle Sizing using Near-forward Scattered Light Signatures", Mechanical Engineering Department, University of Minnesota, Minneapolis, MN, May, 1991.

6. E. D. Hirleman, "Single Particle Sizing using Scattered Light", Mechanical Engineering Department, University of Minnesota, Minneapolis, MN, May, 1991.

7. E. D. Hirleman, "Multiple Scattering and the Fraunhofer Diffraction Particle Sizing Problem", Mechanical Engineering Department, University of Minnesota, Minneapolis, MN, May, 1991.

8. E. D. Hirleman, "Laser Techniques for Simultaneous Particle Size and Velocity Measurements", Mechanical Engineering Department, University of Minnesota, Minneapolis, MN, May, 1991.

9. E. D. Hirleman, "Characterization of Particles on Surfaces using Light Scattering", Mechanical Engineering Department, University of Minnesota, Minneapolis, MN, May, 1991.

VII. PATENTS

1. E.D. Hirleman, "Programmable Detector Array Configuration for Fraunhofer Diffraction Particle Sizing Instruments". AF Invention No. 18,399 Filed for Patent Serial No. 266,952 by Hanscom Patent Prosecution Office, Department of the Air Force. U.S. Patent No. 5,007,737, issued in 1991, assigned to the U.S. Air Force.

VIII. SUMMARY OF IMPORTANT TECHNICAL CONTRIBUTIONS

1. Development of the binary particle-phase fluidized bed concept. This idea, combined with refractive-index matching, will allow the bed to be fluid-dynamically very dense (with interparticle spacings on the order of two diameters as required for stable operation) but optically less thick (with interparticle spacings greater than five diameters where independent, as opposed to dependent, multiple scattering is in effect).

2. Experimental characterization of the performance (edge effects, uniformity, and contrast ratio) of programmable optical shutter arrays for use in multi-angle interrogation of optically thick media. References [6,7, and 8].

From Proceedings of the 2nd International Congress on Optical Particle Sizing, March 5-8, 1990, Tempe, AZ.

A GENERAL SOLUTION TO INVERSE FRAUNHOFER DIFFRACTION PARTICLE SIZING IN MULTIPLE SCATTERING ENVIRONMENTS: EXPERIMENT

Steve B. Kenney and E. Dan Hirleman
Mechanical and Aerospace Engineering Department
Arizona State University
Tempe, AZ 85287-6106

One of the more difficult remaining challenges in the field of optical particle sizing is the characterization of particle size distributions of optically thick, multiple scattering media. In a previous paper [1], a theoretical approach to solving the *forward* problem (i.e. calculation of the scattering signature given the particle size distribution) for the case of near-forward scattering by particles large compared to the wavelength in optically thick media was presented. A subsequent paper included in this Congress [2] is concerned with the corresponding *inverse* problem, i.e. that of estimating the size distribution function of an ensemble of large particles using mathematical inversion of the near-forward optical scattering properties of the optically thick medium. In this paper we discuss the experimental approach which will be used to verify the theoretical developments.

The inverse scattering problem for *single* scattering requires at least n measurements (which is equivalent to specifying n equations) to solve for n unknowns, where the unknowns are the quantity of particles in n size classes. The n measurements are the amounts of light scattered into various scattering angles. Conventional Fraunhofer diffraction systems use a collimated (incident angle of zero) interrogation laser beam, but incident light at any near-forward angle could in fact be used. The optical system of Fig. 1 generates incident (conical) beams of various angles, and for each incident cone n scattering measurements (i.e. at n detectors) could be made. Thus, the system in Fig. 1 could theoretically provide enough measurements to support n *independent* solutions to the n by n single scattering system. The optical system in Fig. 1 system uses transmission mode spatial light modulators as discussed by Dellenback and Hirleman [3].

In optically thick media, the inverse problem is significantly complicated because the light which eventually reaches the detectors has, in general, undergone more than one scattering event. In other words, the single scattering signature (which can be modeled relatively easily) is perturbed or altered by the additional (multiple) scattering events which occur after the light leaves the first scattering event on its way to a detector. Additional unknowns are thereby introduced, specifically variables which determine or predict the expected fate of light which would have reached each of the various detectors if not for the intervening thick medium. Now since light originally traveling at a scattering angle corresponding to say the jth detector could be rescattered into n other detectors, one can define n^2 unknowns necessary to model the n-angle scattering behavior of an optically thick medium. In contrast, the single scattering medium required only n equations and n unknowns. Clearly then additional measurements are needed to characterize a multiple scattering medium, and the system in Fig. 1 can provide n^2 independent measurements (each of n incident light cones scattered to n detectors). After the n^2 measurements are taken via Fig. 1, an n^2 by n^2 system of equations must effectively be solved to determine the particle size distribution.

It has been shown [2] that the inverse problem for multiple scattering, in the case of near-forward scattering, can involve the on-line measurement of the multiple scattering redistribution matrix $\mathbf{H_m}$ defined by:

$$\mathbf{S_m} = \mathbf{H_m} \cdot \mathbf{S_0} \tag{1}$$

where S_0 is a vector defining the irradiance of incident light in n angles, and S_m is a vector defining the angular distribution of irradiance of the (multiple-scattered) light exiting the medium. The scattering redistribution matrix H_m such that the matrix element in the ith row and the jth column $H_m(i,j)$ is the gain or efficiency with which optical energy incident in the jth angle or direction is redistributed by the medium into the ith direction. Now we also know [2]:

$$\mathbf{H_m} \lim \exp(-b) \cdot \exp(a_f b \cdot \mathbf{H}) \tag{2}$$

where a_f and b are the forward-scattering albedo and the optical depth respectively and H is a n by n redistribution matrix valid for single scattering. Now a conventional diffraction system under multiple scattering conditions will measure a signature proportional to the first column of H_m, and only for small b are H and H_m equivalent. But H can be determined from measured H_m using:

$$\mathbf{H} = \exp(b) / (a_f b) \cdot \ln(\mathbf{H_m}) \tag{3}$$

The n^2 terms of H_m are measured using Eq. (1) by illuminating the medium using n different S_0 vectors (i.e. n different hollow cones of incident illumination) and measuring the scattering signature on n different detectors for each incidence case. Then H is obtained from Eq. (3) which in effect amounts to "reaching into the medium" and determining the scattering signature that is present after just one scattering event has taken place. Once the single scattering properties of the medium are known, the inverse problem can be solved using an array of methods discussed in the literature; see Koo [4] for references.

Optical System

Experimental verification of the algorithm for inverse scattering under multiple scattering conditions requires an experimental apparatus where the optical density and particle size distribution of the medium can be carefully controlled. In both the numerical and experimental studies performed here we use NBS standard reference material (SRM) 1003A as the particle size distribution. In the first experiments we used a optical cell with a magnetic stirring system, and dispersed the SRM 1003a particles in water in the cell. The theoretical optical density was proportional to particle concentration assuming that the particles were uniformly distributed in the cell. Particle concentration in the liquid was varied to produce particle fields of different optical thicknesses. Stirred cells do have potential problems in that the centrifuge effect can cause both size and spatial segregation of the particles.

The generation of hollow cones of illumination is performed using a spatial light modulator operated in the transmission mode. The custom device has thirty-two semicircular ring-shaped apertures which can be individually addressed. The ring geometries follow the optimal scaling law discussed by Hirleman [5]. Activating any ring element causes that element to rotate the polarization vector of the transmitted light relative to that of light passing through the unactivated elements. A polarizing element behind the ring window array then preferentially blocks light which has not been rotated. This in effect produces conical shells of light passing through the transmission mask, which in turn produce conical shells of light at the back focal plane of the lens. Cycling through the ring elements produces a sequence of cones of light of different included angles. A matched device at the back focal plane of the collection lens allows measurement of the n^2 elements of **H**.

Particle Flow System

A fluidized bed was designed to create a sample volume in which the particle concentration could be easily varied. A schematic of the experimental apparatus is shown in Fig. 2. Initially, the particles to be sized lie on a stainless steel mesh at the bottom of the fluidizing tube. If a fluid in laminar flow is passed upwards through the tube and past the particles a critical velocity will be reached when the viscous frictional and drag forces equal the weight of the particles in the fluid stream. As the flow rate is increased the bed expands. For beds of liquid-solid composition the bed expands uniformly and the concentration of solid particles is evenly distributed throughout the bed [6]. Therefore, varying optical depths can be produced simply by changing the flow rate of the fluid.

A 0.2mm filter is placed in the line to keep unwanted foreign material from entering the fluidizing tube. To achieve a uniform flow across the cross-sectional area a packed bed of glass beads (6.54mm diameter) was inserted before the fluidizing tube entrance. Optical windows with anti-reflection coatings are mounted near the bottom of the fluidized tube on opposite sides. The incident laser light is passed through the window and the light scattered by the suspended particles is focused and collected on the other side. A rectangular window running the length of the fluidizing tube is used to determine the height of the bed from which the particle concentration can be calculated. To ensure uniform flow all windows are mounted flush to the inside surface.

Results

Experimental results obtained with the multiple scattering cell apparatus discussed above are shown in Fig. 3. Here the measured data for two columns of the $\mathbf{H_m}$ matrix are plotted against the calculated (theoretical) signatures coupled with the successive order multiple scattering model. The data show reasonable agreement, and, based on the theoretical inversion studies in the presence of noise [1], it appears that reconstructions for reasonable numbers of degrees of freedom will be possible. Experiments to characterize the full $\mathbf{H_m}$ matrix are underway.

References

1. E. D. Hirleman, "Modeling of Multiple Scattering Effects in Fraunhofer Diffraction Particle Size Analysis," *Particle and Particulate Systems Characterization*, V. 5, pp. 57-65, 1988.
2. E. D. Hirleman, "A General Solution to Inverse Fraunhofer Diffraction Particle Sizing in Multiple Scattering Environments: Theory", Proceedings of the 2nd International Congress on Optical Particle Sizing, Arizona State University, Tempe, AZ, March 5-8, 1990
3. E. D. Hirleman and P. A. Dellenback, "Adaptive Fraunhofer Diffraction Particle Sizing Instrument Using a Spatial Light Modulator", *Applied Optics*, Vol 28, pp. 4870-4878 (1989).
4. J. H. Koo, "Particle Size Analysis using integral transform techniques on Fraunhofer diffraction patterns", Ph.D. dissertation, George Washington University and Arizona State University, 1987.
5. E. D. Hirleman, "Optimal Scaling for Fraunhofer Diffraction Particle Sizing Instruments," *Part. Char.*, V. 4, pp. 128-133 (1988).
6. J. F. Davidson, R. Clift, and D. Harrison, *Fluidization*, Academic Press, Orlando (1985).

Acknowledgements

This research was sponsored by the Air Force Office of Scientific Research, Air Force Systems Command, USAF, under Grant Number AFOSR-84-0187, Dr. Julian Tishkoff, program manager. The U.S. Government is authorized to reproduce and distribute reprints for Governmental purposes notwithstanding any copyright notation thereon.

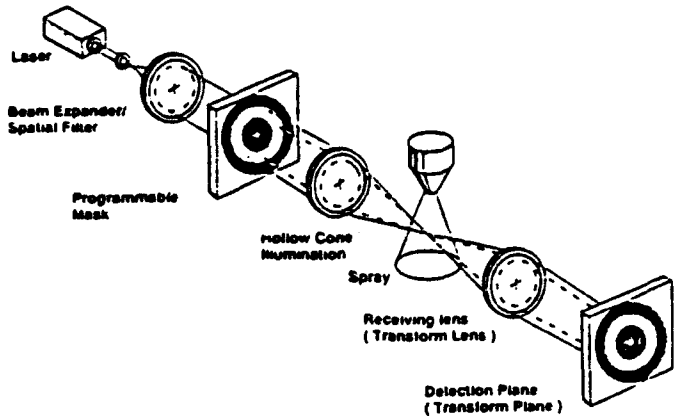

Fig. 1. Schematic of a next-generation laser diffraction particle sizing instrument which allows multi-angle interrogation and multi-angle scattering measurements. The programmable mask creates annular ring of light which are converted into cone of light of varying angles to illuminate the particle field.

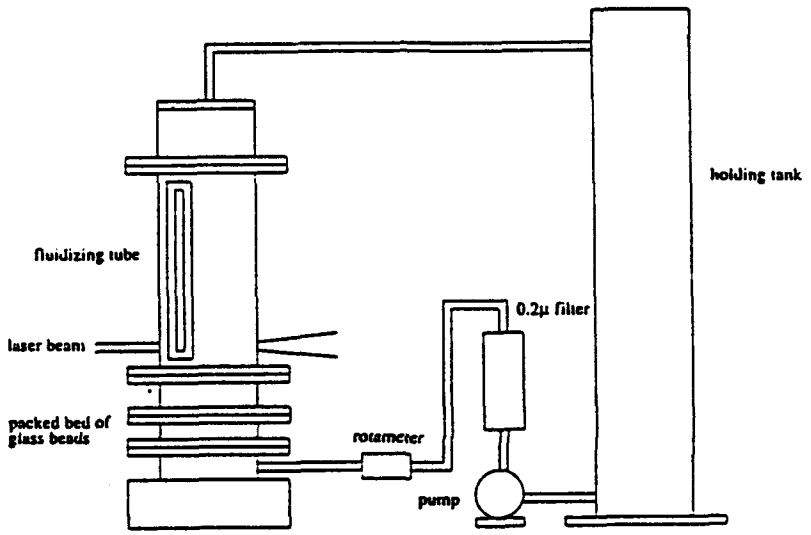

Fig. 2. Schemtic of fluidized bed system.

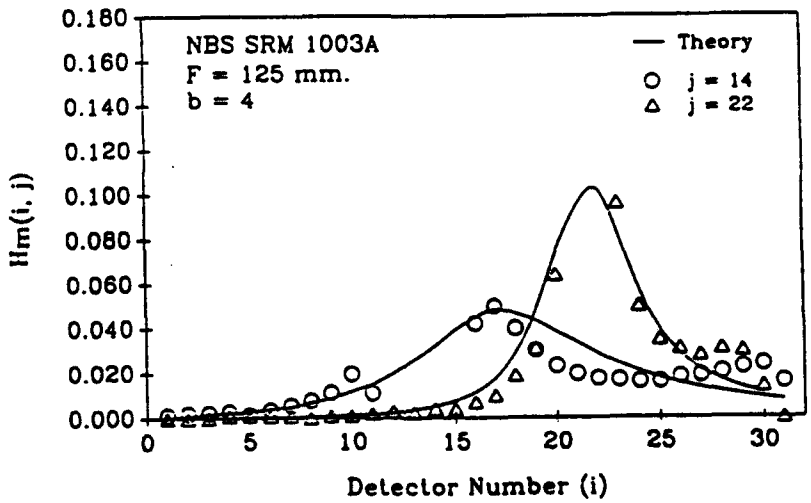

Fig. 3. Measured and predicted data for two columns of the multiple scattering redistribution matrix H_{mr}. The data are for NBS SRM 1003A for a laser diffraction system with an RSI Inc. ring detector and a transform lens with f = 125 mm. The j values correspond to ring detector numbers (0.0162 and 0.0434 rad for rings 14 and 22 respectively).

PROCEEDINGS REPRINT

SPIE–The International Society for Optical Engineering

Reprinted from

Sensors and Sensor Integration

4 April 1991
Orlando, Florida

Volume 1480

Edge effects in silicon photodiode arrays

S. B. Kenney and E. Dan Hirleman
Mechanical and Aerospace Engineering Department
Arizona State University
Tempe, AZ 85287-6106

ABSTRACT

Photodiode arrays used in laser diffraction particle sizing instruments must be calibrated to account for detector-to-detector variations in sensitivity. We have calibrated an Insitec EPCS-P ring detector (planar-diffused, p on n silicon photodiode array) by scanning a focussed laser beam across the detector surface. A deconvolution of the known intensity distribution of the laser beam from the measured signal resulted in detector response as a function of position. Detector response was approximately constant over the region of the ideal active detector and it decreased exponentially in the region beyond the ideal detector boundary. A diffusion length constant of 50μm gave the best fit to the measured data. Theoretical predictions of calibration factors based on measured detector response agreed reasonably well with Malvern and Insitec calibration factors obtained from the traditional uniform light illumination method. This indicates that edge effects in different ring detectors are similar.

1. INTRODUCTION

Many optical processing systems require an array of photodetectors to measure photon flux at the focal plane. We define a detector as a device that converts electromagnetic radiation into an electrical signal. The magnitude of the electrical signal is directly related to the photon flux incident on the device. Photodetectors have been commercially available for some time in 1-D and 2-D arrays of various element shapes. Future improvements in system performance, from a detector standpoint, will include larger arrays, increased speed and dynamic range, and higher resolution.[1] Higher resolution translates into smaller elements, and their associated problems such as (1) crosstalk, the generation of signals at elements other than the one being illuminated and (2) sensitivity, or the unequal response of elements to the same electromagnetic flux. On a smaller scale, differences in element to element sensitivity result directly from the spatial nonuniform response over each element area.[2] This response nonuniformity is due to conditions such as imperfections in the crystalline lattice, variations in doping density, dominant modes of electron-hole transport (diffusion or drift), and surface defects and contamination.

To account for nonuniformities, detector signals are often corrected by multiplying the signal by a predetermined constant. These correction factors are determined empirically by exposing the detectors to one or more uniform irradiance levels.[3] This procedure compensates for relative pixel to pixel sensitivity differences, but does not yield any information on spatial, intra-pixel responsivity variations. Generally, the most dramatic variation in spatial responsivity occurs near the edge or boundary of the detector. As elements become smaller, the responsivity near the element edges has a more pronounced effect on the overall sensitivity of the element. The "edge effect", or responsivity near the element edge, is the topic of this paper, particularly as to how the edge effect impacts log-scaled, annular, semi-circular shaped detector arrays.

An example of an application of photodiode arrays is their use in particle sizing instruments[4] based on near forward scattering signatures. Scattering signatures are collected by a detector array and are processed by a mathematical inversion scheme to determine the size distribution. Embedded in the solution is an assumed detector array response. Consequently, one of the limits on the accuracy of the size distribution solution is proper estimation of the detector array sensitivity.[5]

In the instrument described above a system matrix is usually assembled assuming a step detector response defined by the detector geometry. An improvement in the matrix accuracy, however, would include a more realistic detector response. Through experiment we have measured the response of a detector at various spatial points with the aid of a focussed laser beam. From the experimental data we have defined a mathematical model that accurately predicts detector response through the boundary region. Also, we show how calibration factors are highly dependent on edge response and that from a theoretical model of the edge response characteristics it is possible to predict calibration factors.

0-8194-0589-2/91/$4.00

2. PHOTODIODE DETECTOR BACKGROUND

A photodiode detector is manufactured from a thin silicon wafer. One side of the wafer is doped with atoms from the third column of the periodic table such as boron, while the other side is doped with atoms from the fifth column, such as phosphorus. Silicon doped with Boron is minus an electron to balance the charge in the crystalline structure and the material is called p-type silicon. This gives the material a slight positive charge, hence the symbol p is used. Likewise, silicon doped with Phosphorus is termed n-type silicon because of the extra electron in the lattice, giving it a slight negative charge.

Between the p and n-type silicon regions exists the p-n junction. When the two types of silicon are brought together the extra electrons from the n-type material diffuse to the p-type to fill up the holes near the Boron atoms. The junction has a width of only a few atoms and a small potential is established due to the extra positive charge at the n boundary and the negative charge at the p boundary.

Silicon atoms readily absorb photon energy. If the absorbed energy is greater than 1.1eV, an electron-hole pair will be created. Pairs created in the depletion region or within a diffusion length constant will be separated by the electric field, leading to current flow in the external circuit. For a p-on-n semiconductor, holes will collect at the front ohmic contact, while electrons will collect at the back ohmic contact. The resulting current is approximately proportional to the total illumination and because of this relationship the photodiode can be used as a light measuring device. (For additional information on the physics of photodiode detectors, see Sze).[6]

3. SIZING INSTRUMENT MATHEMATICAL BACKGROUND

Scattering measurements in laser diffraction instruments are typically made with annular ring shaped detectors which cover a finite range of scattering angles as determined by the detector apertures. It is convenient to assign a particular scattering angle θ_i to represent the range of scattering angles in the aperture. The detection process can be represented as:

$$I_w(\theta_i) = \int_0^\infty w_\theta(\theta,\theta_i)\, i(\theta)\, d\theta \qquad (1)$$

where the weighting function $w_\theta(\theta,\theta_i)$ describes the relative responsivity variations across the detector and $I_w(\theta_i)$ is representative of the signal obtained from the ith discrete detector (the subscript w indicates a dependence on the weighting function). The azimuthal, or φ dependence on the responsivity variations are significantly less important than the θ effects, and have been neglected. $i(\theta)$ is the intensity (W/sr) scattered at near-forward scattering angles θ. The weighting function w_θ is what is to be determined experimentally. It is also noted that the particle distribution should also be discretized in a manner similar to that used for the scattering intensity.[7] In that case we obtain a system of m_θ equations in m_α (α is the size parameter) unknowns where m_θ is the number of discrete detectors and m_α is the number of discrete size classes. The linear system is written as:

$$\mathbf{I} = \mathbf{K} \cdot \mathbf{N} \qquad (2)$$

In Eq. (2) the m_θ elements of the vector I are $I_w(\theta_i)$ as given by Eq. (1); the m_α elements of N contain the bth partial moments of the number of particles in the size class; and K is the instrument or system matrix whereby element K_{ij} represents the diffraction contribution of a unit measure of particles in the jth size class onto the ith detector. The elements of K are given by:

$$K_{ij} = \int_0^\infty \int_0^\infty k_b(\alpha,\theta_i)\, w_\alpha(\alpha,\alpha_j)\, w_\theta(\theta,\theta_i)\, d\alpha\, d\theta \qquad (3)$$

where $w_\alpha(\alpha,\alpha_j)$ is a weighting function for the jth size class and $k_b(\alpha,\theta_i)$ is a general scattering function which gives the scattering contribution of a unit quantity of particles of size α into angle θ. Now the solution or measured particle size distribution indicated by N in Eq. (2) can in theory be obtained by inverting the matrix K.

4. EXPERIMENTAL APPARATUS AND PROCEDURE

The experimental apparatus consisted of a laser diffraction particle sizing instrument (Fig. 1). A laser beam is spatially filtered, expanded and collimated to a few millimeter $1/e^2$ diameter. Particles within the collimated beam scatter light which is collected by a receiving lens and refracted onto the detector plane. A commercially available Insitec detector and associated electronics were used in the experiment. The layout of the Insitec detector is well-suited for examining detector response, given its odd numbered rings on one half of the detector and even numbered rings on the other (Fig. 2). This design has large non-responsive sections between adjacent rings, which provides good isolation between adjacent detectors.

The Insitec detector was mounted in a cantilevered position on a programmable x-y translation stage which moved in a plane normal to the beam axis. A HeNe laser beam was focussed to a $1/e^2$ spot 25μm in diameter and the spot was positioned in the small hole in the center of the detector. (The hole allows the strong unscattered light at the center of the detector to pass through, thereby reducing stray reflections and inner ring cross-talk). Coarse centering was performed by moving the detector until the light reflecting off the region surrounding the hole disappeared (indicating the light was passing through the hole). The beam power was adjusted so that when the laser was positioned in the middle of an active detector the resultant signal was just below saturation level. Several runs were made by scanning across the entire detector on a line passing through the center in one direction and then rotating the detector 90 degrees and repeating the scan in the other direction. Signals were recorded at 1μm increments and the entire experimental apparatus was shielded from stray room light.

Before scanning the detector, the rings were examined under a microscope. Three distinct regions were noticed which are shown in Fig. 3 and are labeled as follows: the ideal responsive or active region (R_{active}), the transition region (gap), and the non-active region (masked). The p-n junction within the active region is also shown, though not to scale. The non-active region between each detector consists of a thin aluminum film which has been deposited to mask the area between detectors. It is assumed that the metal helps block radiation so that masked regions are not responsive. Though Fig. 3 shows just one detector, all detectors were examined and found to be similar.

To measure the gap width, the detector was placed on a two-axis translation stage that was coupled to LED displays showing relative stage position. The resolution of the display was 1μm. A camera connected to a 19-inch TV screen was mounted on the microscope which allowed for easy visual inspection of the object. A small piece of tape was placed on the screen to mark the starting and ending points for various features. An inner gap edge was visually lined up with an imaginary tangent line on the edge that would be parallel to the tape. The stages were moved until the outer gap edge was reached and the difference between stage positions was recorded. In this manner the width of each gap, (both inner and outer per detector) was determined.

5. RESULTS AND DISCUSSION

The average gap width was approximately 8μm (results from all detector rings can be found in Table 1). The largest measured gap width was 10μm while the smallest gap width was 6μm, though most widths were 8μm. The table begins with detector 5 because the first four inner rings were damaged when a hole was laser drilled through the detector center. Also included in Table 1 is the visual width of the Insitec detectors (from microscope).

Fig. 4 displays the individual ring signal vs. radial distance for the first five inner odd rings. The rectangular boxes represent the specified width of the detectors and therefore the ideal top hat response distribution, while the curves represent the measured signal. The measured signal is a convolution of the detector spatial response and the Gaussian intensity profile of the laser beam. Since the measured curves are centered around the theoretical points, it was concluded that the laser beam was approximately centered about the detector, which also confirms the accuracy of the stage motion. The maximum signal is close to 8 volts, however this value is not quite reached on rings 4 and 5 because the width of these rings is less than twice the beam width, (where twice the beam width represents more than 99% of the total beam energy). Also, overlap between rings occurs because of the beam width and edge effects resulting from electron hole pair and photon diffusion. Note how overlap decreases with increasing ring size, which is due to the larger regions of non-responsive area between rings. The curves appear smooth except for the saturation region where small deviations in signal are noticed. It should be mentioned that 1000 signals are averaged at each position.

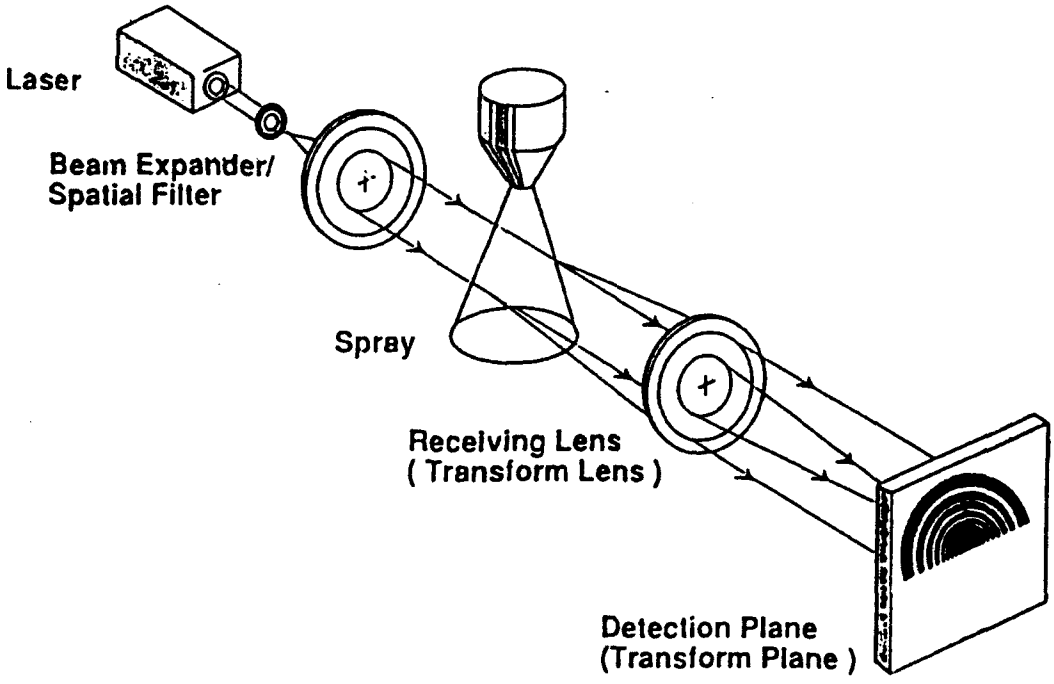

Fig. 1. Schematic of laser diffraction particle sizing system.

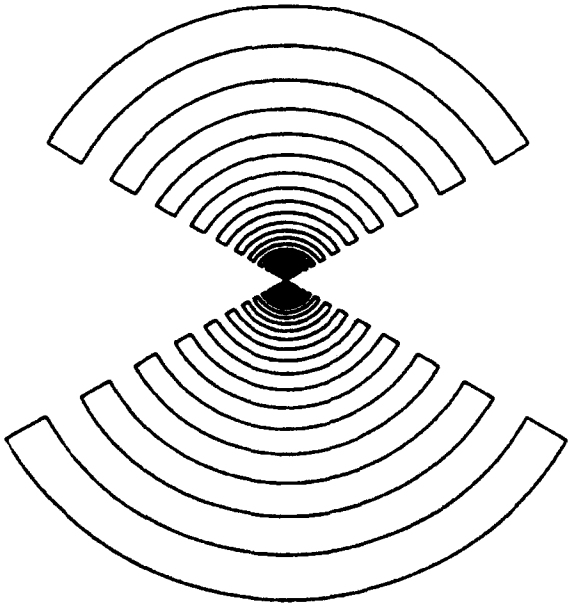

Fig. 2. Insitec detector geometry showing 32 ring photodiode array detector. Odd numbered rings are found on the upper half of the detector and even numbered ones are located on the lower half.

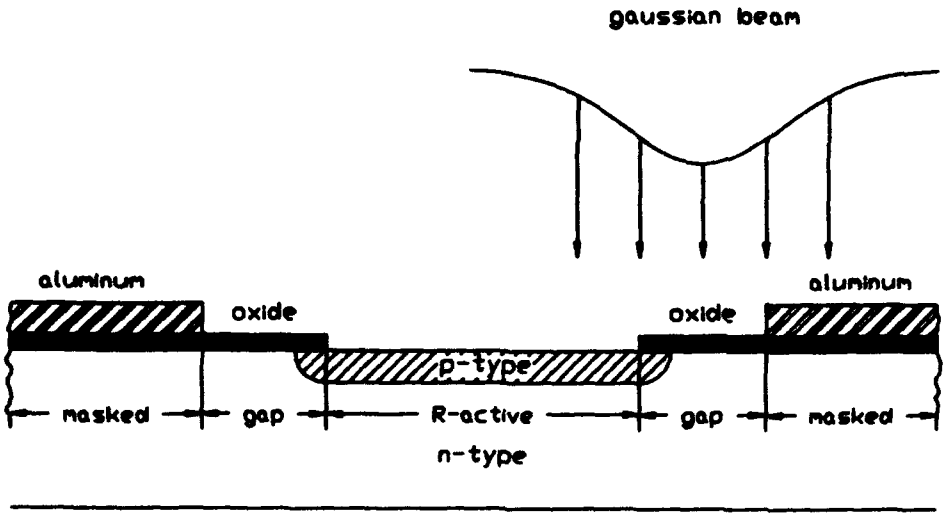

Fig. 3. Cross section of an Insitec photodiode detector showing the ideal responsive region (R-active), the transition region (gap), and the non-active region (masked).

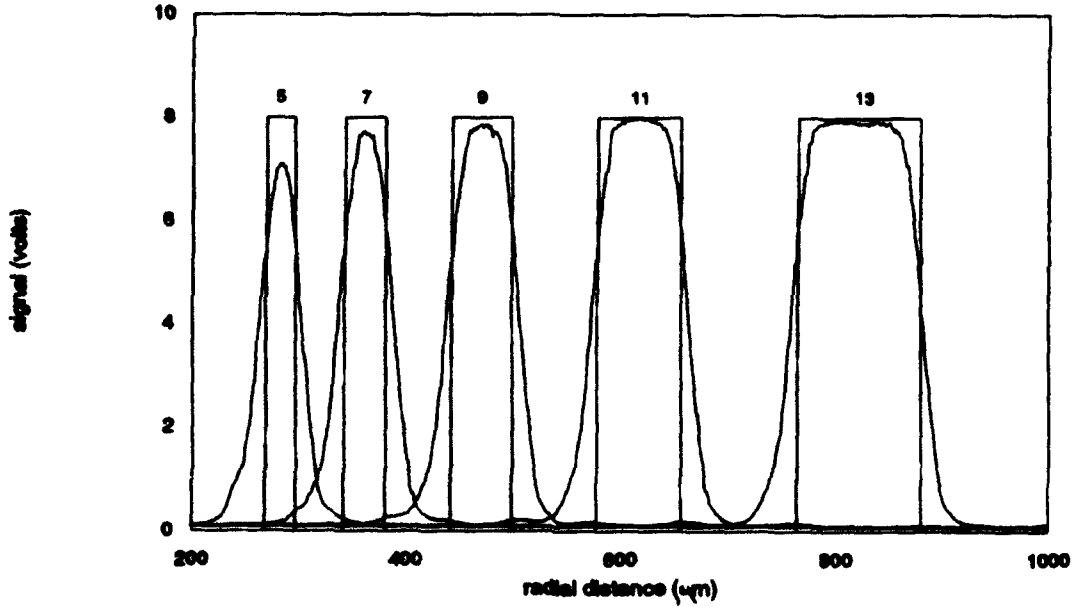

Fig. 4. Plot of detector signal vs. radial distance for five inner odd rings. The rectangles represent the specified detector dimensions. The curves are the signals resulting from a $1/e^2$ 25μm diameter laser beam of wavelength 0.6328μm. Measurements were made at 1μm increments and the corresponding signal at each position is an average of 1000 data points.

Table I

Insitec ideal detector width and gap width. Visual dimensions were acquired by viewing the detector under a microscope.

Detector	Visual detector width (μm)	Visual gap width inner (μm)	outer (μm)
5	27	7	7
6	29	8	8
7	38	7	8
8	47	7	6
9	55	8	8
10	65	7	8
11	77	7	8
12	92	8	8
13	108	7	7
14	127	7	7
15	149	8	9
16	177	8	9
17	209	8	6
18	244	7	7
19	285	7	8
20	333	10	6
21	392	7	8
22	455	9	10
23	532	8	10
24	625	8	8
25	730	7	8
26	855	8	7
27	997	8	9
28	1165	8	7
29	1361	10	8
30	1586	7	9
31	1855	7	8
average		8	8

In order to be able to calculate w_θ for use in Eq. (1) it is necessary to model the gap response. This response can be estimated by deconvolving the measured signal from the known Gaussian intensity profile of the laser beam. After several runs were taken of the inner odd rings (results of rings 11,13,15) an average response of the gap region was calculated by first determining the average signal for each ring at each 1μm position (over a 100μm distance) and then superimposing the profiles from the 3 outer edges (5 runs for each edge) to calculate an overall average. This average gap response curve is shown in Fig. 5.

Initial insight into a possible model for the gap response is found by looking for symmetry within the curve. Fig. 6 shows two curves labeled upper and lower. The upper curve is the first 50μm of the average edge response curve normalized to one, while the lower curve is obtained by "inverting" the last 50μm of the average edge curve. The lower curve is found by subtracting 1 from each lower signal and superimposing the new curve onto the upper curve. It is apparent from Fig. 6 that a certain degree of symmetry exists. This is especially true for the signal values associated with a position between 30μm and 50μm. For radial positions less than 30μm there is slight discrepancy between curves which is most likely attributable to

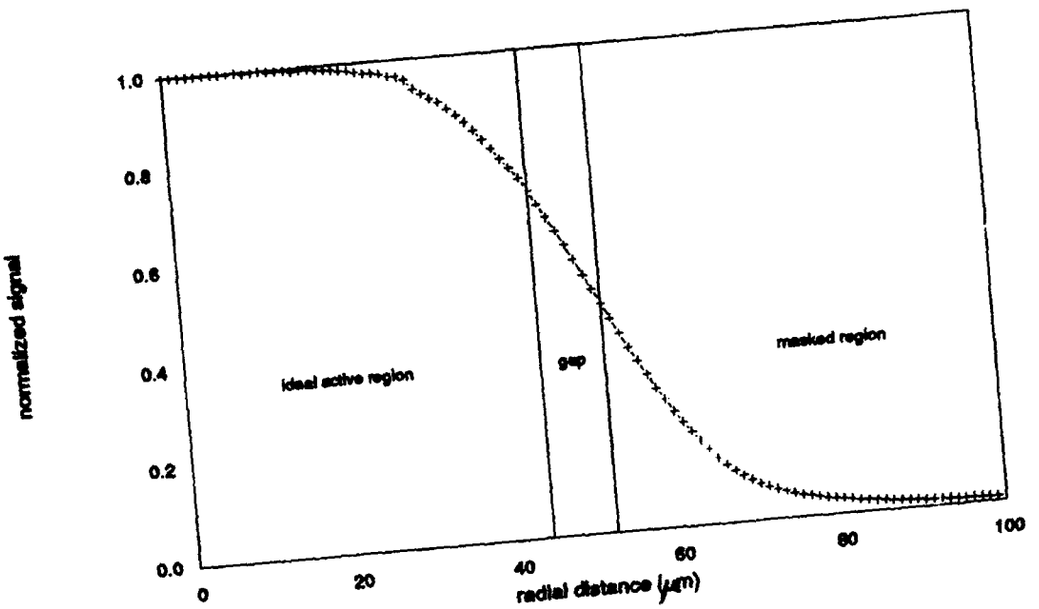

Fig. 5. Plot of the average edge signal of rings 11, 13, and 15 resulting from a 25μm diameter $1/e^2$ Gaussian laser beam vs. relative distance. The signals of the three rings are superimposed to form one curve. The three regions of the detector are as labeled on the figure.

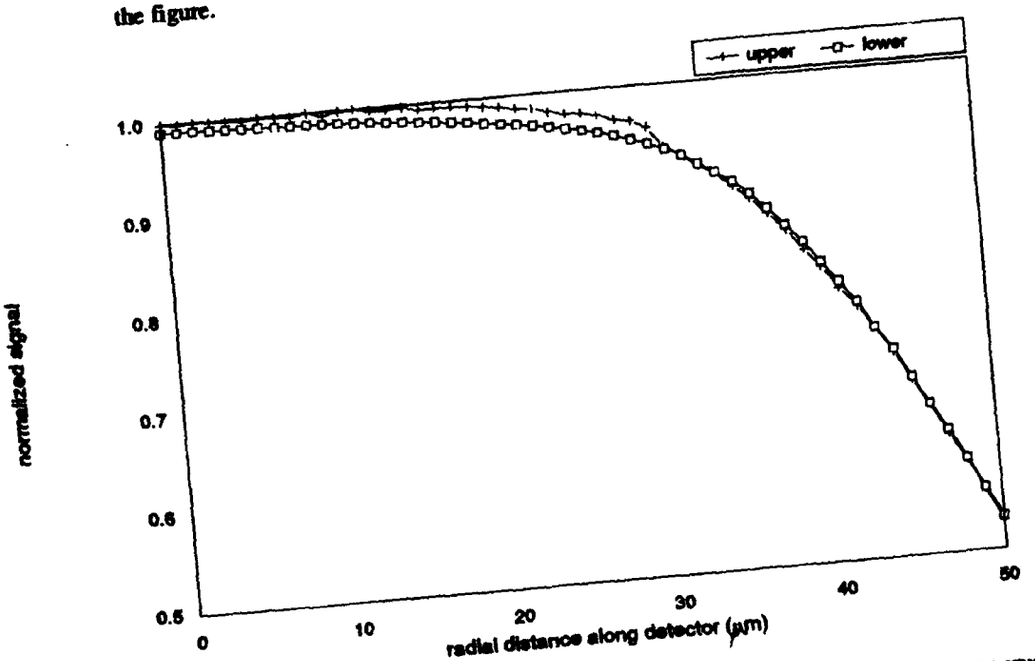

Fig. 6. Plot showing the symmetry of the average edge curve of Fig. 5. The upper curve is the first 50μm of the average edge response curve normalized to one. The lower curve is the last 50μm of the curve inverted and positioned over the first 50μm.

random noise or reflections from the mask affecting the ring output, although the background signal which contains most of the noise has already been subtracted from the total signal. There is a residual signal obtained when the beam is illuminating the mask even though we would expect no response.

The symmetry present in the curve points to a potential model based on a simple function, most likely exponential. A logical model to predict the gap response would include uniform response over the idealized detector region, decaying exponential response over the 8μm gap width and no response in the masked or non-responsive region. Photons incident on the gap region are absorbed by the silicon where they create electron-hole pairs. The electron-hole pairs begin diffusing through the material until they either reach the p-n junction, where there is a possibility that they will contribute to the overall current, or, they lose their energy through collisions and recombine. As far as this model is concerned only one parameter will need to be determined, the "diffusion length constant" governing the decaying exponential.

However, it should be mentioned that when convolving the Gaussian beam with the gap response function the value of the diffusion length constant has only a slight impact on the slope of the curve, thereby making it difficult to estimate the proper value of the constant to match the measured data. Fig. 7 confirms this observation, where three curves representing the same beam diameter, but different diffusion length constants are displayed. As can be imagined the gap response resulting from different diffusion constants is highly variable, yet because the beam width is much greater than the gap width the slopes of the curves are nearly equal. If the beam width was less than the edge width then the slopes of the three curves would be much different. Furthermore, if the beam was reduced to a point source then the response would simply be the exponential itself. However, even with large beam widths a difference exists between the curves. The results are sensitive to diffusion length in that the curves expand with increasing diffusion length constant.

Since the specified width of each detector is known, a theoretical calculation could use diffusion constants as a means to expand or contract the curve to fit the measured data and determine the diffusion length constant. First, the total laser power in the Gaussian laser beam is normalized to one and the beam is moved in one micron increments over the ideal, gap, and masked regions. At each position the expected signal is calculated by convolving the response function (assuming a diffusion length) with the Gaussian beam intensity. (As can be seen from Fig. 2 there are instances when the width of the beam covers all three regions of the detector.) These values are then compared to the measured data to find the diffusion length constant that provides the best fit.

Experimental data from ring 9 were compared to theoretical calculations based on different diffusion length constants. Assumed values in the theoretical calculations include a 25μm Gaussian intensity profile diameter laser beam, gap width of 8μm, and total detector width obtained from visual inspection. Results showed that a diffusion length constant of 50μm gave the best fit between experimental and theoretical values. A plot of ring 9 normalized signal vs. distance is found in Fig. 8, and as can be seen from the graph the fit is quite good. Diffusion lengths are fundamental characteristics of semiconductor devices and many of the techniques used to measure them are reviewed by Schroder.[8] Our measured diffusion length of 50μm ± 10μm is consistent with typical values for p-n junction devices. As a test for the model, comparisons were made between experimental and measured results for many of the other rings and similar results were noted. Thus, it was concluded that a simple exponential function appears to adequately predict the edge response of the Insitec ring detector. The weighting function over the width of an edge can be written as:

$$w_{\theta edge} = \rho/\rho_0 = e^{-x/xd} \qquad (4)$$

where $\rho(\theta)$ is the local responsivity, ρ_0 is the maximum responsivity in the ideal active region of the detector, xd is the diffusion length constant, and x is the position measured from the ideal edge into the gap. Now that the weighting function w_θ has been determined a new instrument matrix K can be calculated by substituting the measured gap weighting function of Eq. (4) into Eq. (3) in place of the usually assumed step function. To quantify the effect of the detector weighting function on the instrument matrix, two matrices were calculated; one assuming a step detector response, the other the actual measured response (and weighting values of 0 and 1 in the masked and idealized regions, respectively). A plot of the difference matrix (element by element) between the two matrices is presented in Fig. 9. The matrices were calculated on a particle area basis with rectangular weighting functions, uniform by volume within-class distributions, and a Fraunhofer diffraction approximation. The surface plot shows almost no change on the outer rings, while the difference between elements increases as ring dimensions decreases. This is expected, as the ratio of edge area to visual detector area is much greater for smaller rings than larger ones.

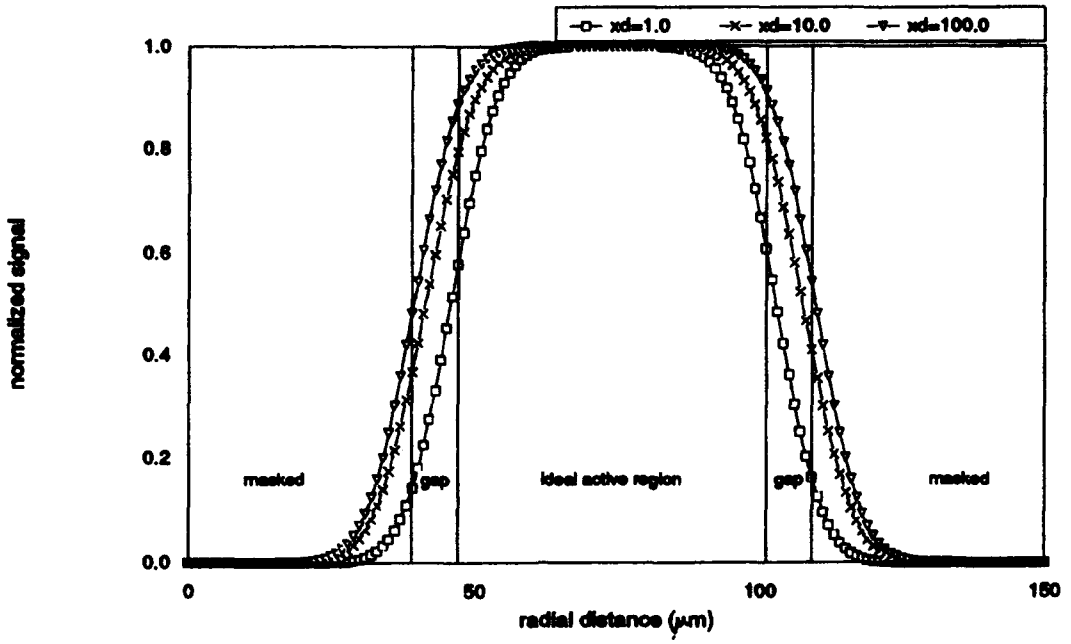

Fig. 7. Plot of theoretical signal curves calculated by convolving a 25μm beam diameter with the theoretical detector response. The specified detector width is 55μm which corresponds to ring 9 of the Insitec detector. Calculations are made with different diffusion length constants as indicated. The ideal active, gap, and masked regions are also indicated on the figure.

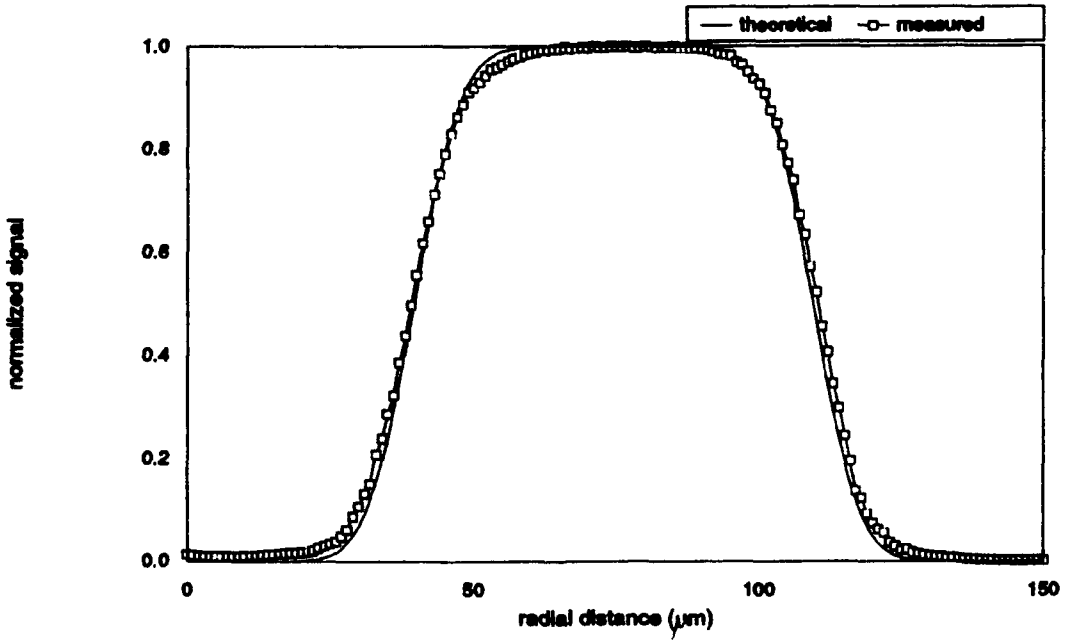

Fig. 8. Comparison of theoretical and measured signal vs. relative distance for ring 9 of the Insitec detector. The theoretical signal was calculated based on a 25μm beam diameter, 8μm edge width, 50μm diffusion length, and 55μm detector width.

It has already been mentioned that it is possible to predict calibration factors based on gap or transition region response as opposed to systematic between-detector variations in the responsivity. The accuracy of the "gap" calculated factors is based on the premise that the major contribution to calibration factors is from gap response. A predicted calibration factor is defined here as the ratio of the ideal detector output to the actual detector output when illuminated with light of uniform intensity. The ideal detector output is calculated by integrating the incident light intensity over the ideal, visual detector area while assuming that the weighting function w_θ is constant and equal to one. The actual detector output is found in the same manner except the area over which the integration is performed includes the gap region and the associated weighting function $w_{\theta edge}$. In equation form we have:

$$C_{pred} = \frac{\int I\, dA}{\int w_\theta\, I\, dA} = \frac{\int dA_{(ideal)}}{\int w_{\theta edge}\, dA_{(gap)} + \int dA_{(ideal)}} \tag{5}$$

where C_{pred} is the predicted calibration factor and I is the intensity (W/m^2).

Traditionally, calibration factors have been determined based on illuminating the detectors with uniform light intensity. We determined two sets of calibration factors for the Insitec detector. One set of factors was calculated using Eq. (5), while the other set was determined using the uniform light method. Results of the two methods are displayed in Fig. 10 along with calibration factors from 3 different[9,10,11] Malvern 2600 instruments determined empirically with the uniform light method. Since the Insitec detector geometry differs slightly from the Malvern detector geometry, the calibration factors are plotted vs. detector width. As is seen from the plot the curves are in reasonable agreement. Noticed trends are that all factors decrease in value as detector area decreases. Consequently, the inner detectors over-respond relative to the outer detectors. Calibration factors determined from Eq. (5) are limited by the fact that experimental data were collected along two lines running through the center of the detector instead of scanning the entire detector surface. Additionally, in Eq. (5) it was assumed that the weighting function equals a constant over the ideal detector region, however, Fig. 4 shows slight variation in this region. One other area of uncertainty which we did not investigate is the ends of each detector. Though we accounted for the end region in the calculations the region is different from the rest of the perimeter regions in that a masked area is not found 8μm from the ideal detector boundary. A drawback to the uniform light method is that linear detector response is assumed with no cross-talk. If either of the above assumptions is not correct then errors in calibration factors will propagate through the remaining factors that need to be determined. This results from the requirement that values acquired from different light levels must be spliced together.[3] Overall, it appears that calibration factors calculated using Eq. (5) compare reasonably well with factors determined with the uniform light method, especially considering the fact that factors are for different detectors from different laboratories.

6. CONCLUSIONS

In conclusion, the transition region response has been measured and modeled for an Insitec detector. A simple exponential with a diffusion length constant of 50μm accurately predicted the experimental data. The detector weighting function has been calculated and incorporated into the instrument matrix K. Calibration factors for the Insitec detector have been predicted based on edge effects and were compared with calibration factors derived from the uniform light source technique. Both methods indicated that the inner rings over-respond relative to the outer, larger rings. It is difficult to conclude which method produces the more accurate results. The uniform light method has the disadvantage that detector signals resulting from several light levels must be measured and the calibration curves spliced together. The gap response model has the disadvantage that it is based on 2-dimensional results and it must be assumed that gap response is axisymmetric. Another independent technique for calculating calibration factors could help verify whether the gap or uniform light source is more accurate. The effect of using the theoretical calibration factors instead of the uniform light source factors would, in general, translate into slightly larger particle sizes because of the higher signals on the inner rings.

7. ACKNOWLEDGMENTS

This research was supported by the Air Force Office of Science Research, Air Force Systems Command, USAF, under grant AFOSR-90-0358, Dr. Julian Tishkoff, program manager. The U.S. government is authorized to reproduce and distribute reprints for governmental purposes notwithstanding any copyright notation thereon.

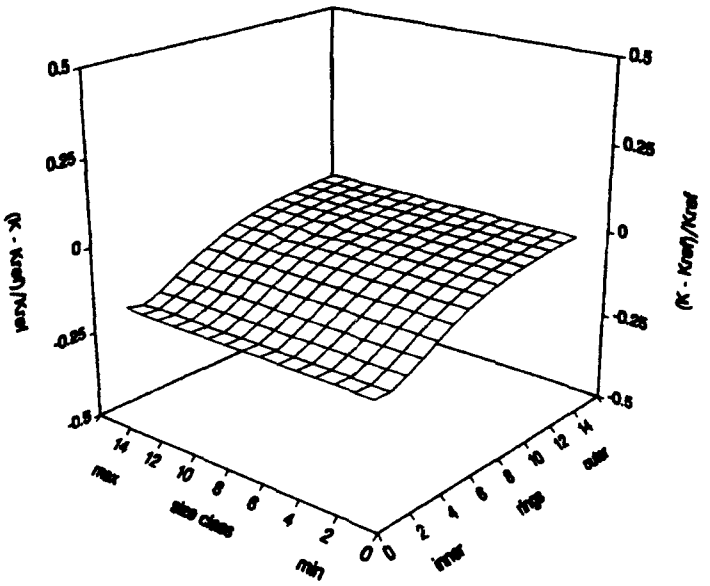

Fig. 9. Plot of the difference matrix between K_{ref} based on a step response detector weighting function and K obtained with theoretical detector response weighting function (which accounts for detector response in the gap region between the mask and idealized detector boundary).

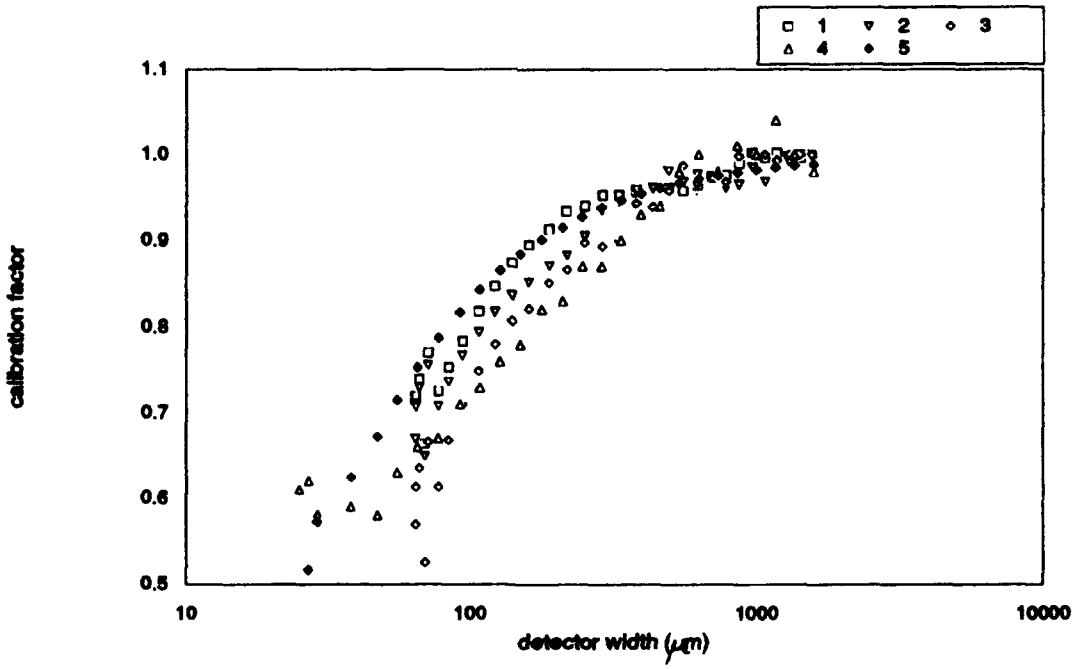

Fig. 10. Plot of calibration factors vs. detector width for various instruments and calibration techniques. The numbers in the legend correspond to the following: 1) Malvern 2600, instrument #1, uniform incoherent illumination.[3,11] 2) Malvern 2600, instrument #2, factory supplied calibration factors.[9] 3) Malvern 2600, instrument #3, uniform incoherent illumination.[10] 4) Insitec, uniform incoherent illumination. 5) Insitec, theoretical predictions based on gap response method.

8. REFERENCES

1. J. N. Lee and A. D. Fisher, "Device Developments for Optical Information Processing," in *Advances in Electronics and Electron Physics*, V. 69, P. W. Hawkes, Ed. Academic Press, San Diego, CA (1987), pp. 115-173.

2. J. Campos, A. Corrons, and A. Pons, "Response Uniformity of Silicon Photodiode," *Applied Optics*, V. 27, pp. 5154-5156 (1989).

3. L. G. Dodge, "Calibration of the Malvern Particle Sizer," *Applied Optics*, V. 23, pp. 2415-2419 (1984).

4. E. D. Hirleman, "Particle Sizing by Optical, Nonimaging Techniques," in Liquid Particle Size Measurement Techniques, STP 848, J. M. Tishkoff, R. D. Ingebo, and J. B. Kennedy, Eds. (American Society of Testing Materials, Philadelphia, 1984), pp. 35-60.

5. E. D. Hirleman, "Uncertainties in Matrix Formulations of the Fraunhofer Diffraction Particle Size Problem., Conference of the Institute of Liquid Atomization and Spray Systems, (1989), Irvine, CA.

6. S. M. Sze, *Physics of Semiconductor Devices*, John Wiley and Sons, New York (1981).

7. E. D. Hirleman, "Optimal Scaling for Fraunhofer Diffraction Particle Sizing Instruments," *Particle Characterization.*, V. 4, pp. 128-133 (1988).

8. D. K. Schroder, *Semiconductor Material and Device Characterization*, John Wiley and Sons, New York, (1990).

9. G. S. Samuelsen, University of California, Irvine, CA (private communication).

10. E. A. Hovenac, NASA Lewis Research Center, Cleveland, Ohio (private communication).

11. L. G. Dodge, Southwest Research Institute, San Antonio, Texas (private communication).

From Proceeding of the Fifth International Conference on Liquid Atomization and Spray Systems, NIST Special Publication 813, U.S. Goverment Printing Office, Washington, DC, 1991.

CALIBRATION FACTORS FOR LASER DIFFRACTION RING DETECTORS: THEORETICAL MODELING

S.B. Kenney and E.D. Hirleman

Mechanical and Aerospace Engineering Department
Arizona State University
Tempe, AZ, U.S.A.

ABSTRACT

Photodiode arrays used in laser diffraction particle sizing instruments must be calibrated to account for detector-to-detector variations in sensitivity. We have calibrated an Insitec EPCS-P detector by scanning a small laser beam across the detector surface. A deconvolution of the known intensity distribution of the laser beam from the measured signal resulted in detector response as a function of position. Detector response was approximately constant over the region of the ideal active detector and it decreased exponentially in the region beyond the ideal detector boundary. A diffusion length constant of 50μm gave the best fit to the measured data. Theoretical predictions of calibration factors based on measured detector response agreed reasonably well with Malvern and Insitec calibration factors obtained from the traditional uniform light illumination method. This indicates that edge effects in ring detectors made by different sources are similar.

INTRODUCTION

Particle sizing instruments based on near forward scattering signatures are commonly used to measure droplet size distributions in sprays [1]. Scattering signatures are collected by the instrument and are processed by a mathematical inversion scheme to determine the size distribution. The equation which models the scattering signature is a classical Fredholm integral equation. This integral equation is often approximated by a linear system of discretized equations and the calculated size distribution is only an approximation of the actual distribution. The corresponding coefficient matrix resulting from discretization contains elements that must be estimated. Two of these components are the distribution of particle size within each size class and detector response characteristics. The ultimate accuracy of the calculated size distribution is limited by the accuracy to which these components are properly estimated.

Since it is the particle size distribution that is sought, it is doubtful that any information on within class size distributions would be known *a priori*. However, it is possible to experimentally probe the detector response. Literature references [2-4] discuss calculation of the scattering matrix assuming an ideal step response at the boundary of detector elements. Any deviation in the actual detector edge response characteristics from this assumed ideal behavior would result in a bias error in the matrix, and hence, also in the calculated size distributions. Further, all scattering matrix calculations reported to date have assumed no detector-to-detector variation in responsivity, the ideal situation. However, since interlaboratory studies [5] highlighted the significant effect of between-detector responsivity variations on the overall accuracy of laser diffraction instruments, calibration factors have been introduced to correct for these between-detector effects. The process of calibrating a photodetector array using uniform illumination [6] can experimentally correct for two effects, 1) spatial variations in the local responsivity (amps/watts) either within or between detectors, and 2) edge effects. Clearly, details of these local effects are masked by the averaging effect of uniform flood illumination. In this paper we are concerned with the details of detector array characteristics on a spatial scale much smaller than the detector dimensions. In particular, we report

experimental measurements of local responsivity both within and at the boundaries of the detector elements. We have used the results to develop a theoretical model for the edge effects and we therefore are able to theoretically predict calibration factors.

MATHEMATICAL FORMULATION

Scattering measurements in laser diffraction instruments are typically made with annular ring shaped detectors which cover a finite range of scattering angles as determined by the detector apertures. It is convenient to assign a particular scattering angle θ_i to represent the range of scattering angles in the ith detector aperture. The detection process can be represented as:

$$I_w(\theta_i) = \int_0^\infty w_\theta(\theta,\theta_i)\, i(\theta)\, d\theta \tag{1}$$

where the weighting function $w_\theta(\theta,\theta_i)$ describes the relative responsivity variations across the detector and $I_w(\theta_i)$ is representative of the signal obtained from the ith discrete detector (the subscript w indicates a dependence on the weighting function). The azimuthal, or φ dependence on the responsivity variations are significantly less important than the θ effects, and have been neglected. $i(\theta)$ is the intensity (W/sr) diffracted at near-forward scattering angles θ. The weighting function w_θ is what is to be determined experimentally. It is also noted that the particle distribution should also be discretized in a manner similar to that used for the scattering intensity [7]. In that case we obtain a system of m_θ equations in m_α (α is the size parameter) unknowns where m_θ is the number of discrete detectors and m_α is the number of discrete size classes. The linear system is written as:

$$I = K \cdot N \tag{2}$$

In Eq. (2) the m_θ elements of the vector I are $I_w(\theta_i)$ as given by Eq. (1); the m_α elements of N contain the bth partial moments of the number of particles in the size class; and K is the instrument or system matrix whereby element K_{ij} represents the diffraction contribution of a unit measure of particles in the jth size class onto the ith detector. The elements of K are given by:

$$K_{ij} = \int_0^\infty \int_0^\infty k_b(\alpha,\theta_i)\, w_\alpha(\alpha,\alpha_j)\, w_\theta(\theta,\theta_i)\, d\alpha\, d\theta \tag{3}$$

where $w_\alpha(\alpha,\alpha_j)$ is a weighting function for the jth size class and $k_b(\alpha,\theta_i)$ is a general scattering function which gives the scattering contribution of a unit quantity of particles of size α into angle θ. The solution or measured particle size distribution indicated by N in Eq. (2) can in theory be obtained by inverting the matrix K.

EXPERIMENTAL PROCEDURE

Fig. 1 shows a schematic for a laser diffraction particle sizing instrument. A laser beam is spatially filtered, expanded and collimated to a few millimeter $1/e^2$ diameter. Particles within the collimated beam scatter light which is collected by a receiving lens and refracted onto the detector plane. A commercially available Insitec particle sizing detector head and electronics were used for the experiment. The layout of the Insitec detector is well-suited for examining detector response, given its odd numbered rings on one half of the detector and even numbered rings on the other. This design has large non-responsive sections between adjacent rings, which provides good isolation between adjacent detectors.

The Insitec detector was mounted in a cantilevered position on a programmable x-y translation stage which moved in a plane normal to the beam axis. A HeNe laser beam was focussed to a $1/e^2$ spot 25μm in diameter and the spot was positioned in the small hole in the center of the detector. (The hole allows the strong unscattered light at the center of the detector to pass through, thereby reducing stray reflections and inner ring cross-talk). Coarse centering was performed by moving the detector until the light reflecting off the region surrounding the hole disappeared (indicating the light was passing through the hole). The beam power was adjusted so that when the laser was positioned in the middle of an active detector the resultant signal was just below the saturation level.

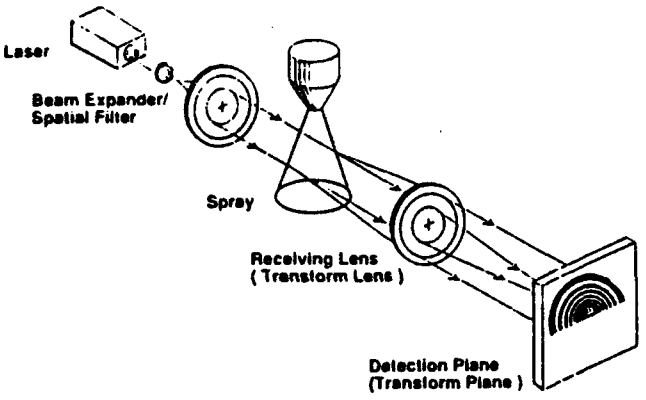

Fig. 1. Schematic of conventional laser diffraction particle sizing system.

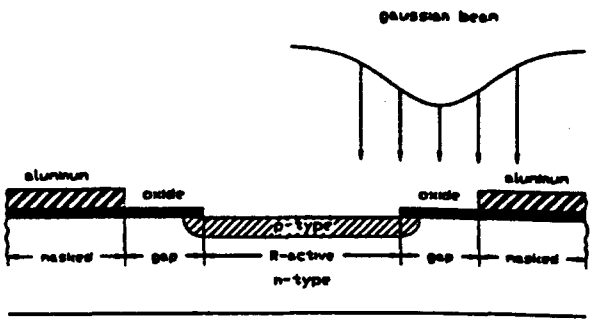

Fig. 2. Cross section of an Insitec photodiode detector showing the ideal responsive region (R-active), the transition region (gap), and the non-active region (masked).

Several runs were made by scanning across the entire detector on a line passing through the center in one direction and then rotating the detector 90 degrees and repeating the scan in the other direction. Signals were recorded at 1μm increments and the entire experimental apparatus was shielded from stray room light.

Before scanning the detector, the rings were examined under a microscope. Three distinct regions were noticed which are shown in Fig. 2 and are labeled as follows: the ideal responsive or active region (R_{active}), the transition region (gap), and the non-active region (masked). Bounding each detector is a thin aluminum film, which has been deposited to cover most of the area between detectors. It is assumed that the metal helps block radiation so that masked regions are not responsive. Though Fig. 2 shows just one detector, all detectors were examined and found to be similar.

To measure the gap width, the detector was placed on a two-axis translation stage that was coupled to LED displays showing relative stage position. The resolution of the display was 1μm. A camera connected to a 19-inch TV screen was mounted on the microscope which allowed for easy visual inspection of the object. A small piece of tape was placed on the screen to mark the starting and ending points for various features. An inner gap edge was visually lined up with an imaginary tangent line on the edge that would be parallel to the tape. The stages were moved until the outer gap edge was reached and the difference between stage positions was recorded. In this manner the width of each gap (both inner and outer per detector), was determined.

RESULTS AND DISCUSSION

The average gap width was approximately 8μm (results from all detector rings can be found in Table 1). The largest measured gap width was 10mm while the smallest gap width was 6mm, though most widths were 8mm. The table begins with detector 5 because the first four inner rings were damaged when a hole was laser drilled through the detector center. Also included in Table 1 is the visual measured width of the Insitec detectors (from microscope).

Fig. 3 displays the individual ring signal vs. radial distance for the first five inner odd-numbered rings. The rectangular boxes represent the specified width of the detectors and therefore the ideal top hat response distribution, while the curves represent the measured signal. The measured signal is a convolution of the detector spatial response and the Gaussian intensity profile of the laser beam. Since the measured curves are centered around the specified points, it was concluded that the laser beam was approximately centered about the detector. The maximum signal is close to 8 volts, however this value is not quite reached on rings 4 and 5 because the width of the rings is less than twice the beam width, (where twice the beam width represents more than 99% of the total beam energy). Also, overlap between rings occurs because of the beam width and edge effects resulting from electron hole pair and photon diffusion. Note how overlap decreases with increasing ring size, which is due to the larger regions of non-responsive area between rings. The curves appear smooth except for the saturation region where small deviations in signal are noticed. It should be mentioned that 1000 signals are averaged at each position.

In order to be able to calculate w_θ for use in Eq. (1) it is necessary to model the gap response. This response can be estimated by deconvolving the measured signal from the known Gaussian intensity profile of the laser beam. After several runs were taken of the inner odd rings (results of rings 11,13,15) an average response in the gap region

Table I

Insitec ideal detector width and gap width. Visual dimensions were acquired by viewing the detector under a microscope.

Detector	Visual detector width (μm)	Visual gap width inner (μm)	outer (μm)
1			
2			
3			
4			
5	27	7	7
6	29	8	8
7	38	7	8
8	47	7	6
9	55	8	8
10	65	7	8
11	77	7	8
12	92	8	8
13	108	7	7
14	127	7	7
15	149	8	9
16	177	8	9
17	209	8	6
18	244	7	7
19	285	7	8
20	333	10	6
21	392	7	8
22	455	9	10
23	532	8	10
24	625	8	8
25	730	7	8
26	855	8	7
27	997	8	9
28	1165	8	7
29	1361	10	8
30	1586	7	9
31	1855	7	8
average		8	8

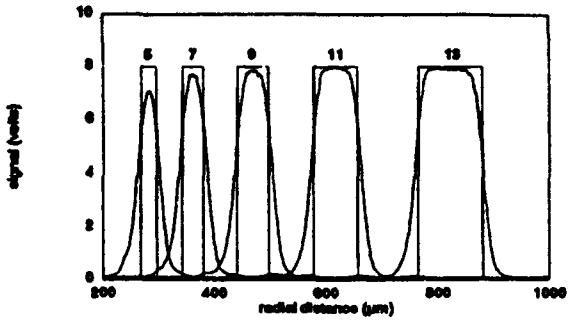

Fig. 3. Plot of detector signal vs. radial distance for five inner odd rings. The rectangles represent the specified detector dimensions. The curves are the signals resulting from a $1/e^2$ 25μm diameter laser beam of wavelength 0.6328μm. Measurements were made at 1μm increments.

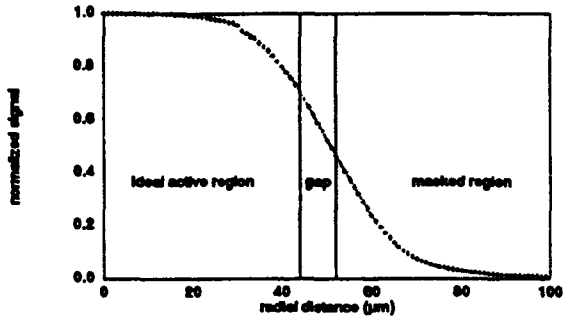

Fig. 4. Plot of the average edge signal of rings 11, 13, and 15 vs. relative distance. The signals of the three rings are superimposed to form one curve.

was calculated by determining the average signal for each ring at each 1μm position (over a 100μm distance) and then superimposing the data to calculate an overall average. This average gap response curve is shown in Fig. 4.

Initial insight into a possible model for the gap response is found by looking for symmetry within Fig. 4. The symmetry present in the curve points to a potential model based on a simple function, most likely exponential. A logical model to predict the gap response based on physical conditions would include uniform response over the idealized detector region, decaying exponential response over the 8μm gap width and no response in the masked or non-responsive region.

Photons incident on the gap region are absorbed by the silicon where they create electron-hole pairs. The electron-hole pairs begin diffusing through the material until they either reach the p-n junction where there is a possibility that they will contribute to the overall current, or they lose their energy through collisions and recombine. For an overview of the physics of photodiode operation see Sze [8]. As far as a model is concerned only one parameter will need to be determined; the "diffusion length constant" governing the decaying exponential.

However, it should be mentioned that when convolving the Gaussian beam with the gap response function the value of the diffusion length constant has only a slight impact on the slope of the curve, thereby making it difficult to estimate the proper value of the constant to match the measured data. Fig. 5 confirms this observation, where three curves representing the same beam diameter, but different diffusion length constants are displayed. As can be imagined the gap response resulting from different diffusion constants is highly variable, yet because the beam width is much greater than the gap width the slopes of the curves are nearly equal. If the beam width was less than the gap width then the slopes of the three curves would be much different. Furthermore, if the beam was reduced to a point source then the response would simply be the exponential itself. However, even with large beam widths a

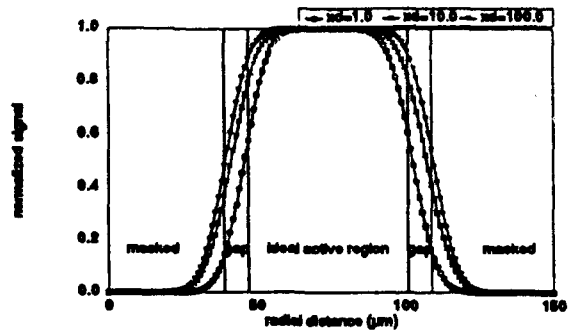

Fig. 5. Plot of theoretical signal curves calculated by convolving a 25μm beam diameter with the theoretical detector response. The specified detector width is 55μm which corresponds to ring 9 of the Insitec detector. Calculations are made with different diffusion length constants as indicated. The ideal active, gap, and masked regions are also indicated on the figure.

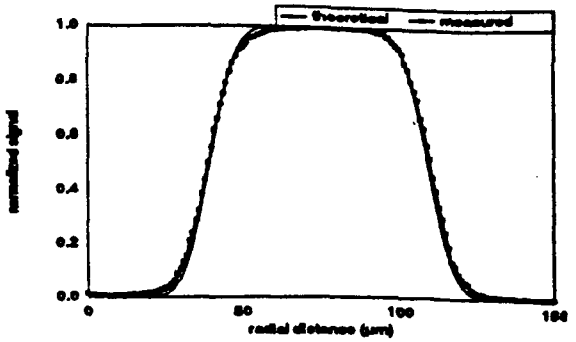

Fig. 6. Comparison of theoretical and measured signal vs. relative distance for ring 9. The theoretical signal was calculated based on a 25μm beam diameter, 8μm edge width, 50μm diffusion length, and 55μm detector width.

difference exists between the curves. The results are sensitive to diffusion length in that the curves expand with increasing diffusion length constant.

Since the specified width of each detector is known, a theoretical calculation could use diffusion constants as a means to expand or contract the curve to match the measured data. First, the total laser power in the Gaussian beam is normalized to one and the beam is moved in one micron increments over the idealized, gap, and masked regions. At each position the expected signal is calculated by convolving the response function (assuming a diffusion length) with the Gaussian beam intensity. (As can be seen from Fig. 2 there are instances when the width of the beam covers all three regions of the detector.) These values are then compared to the measured data to find the diffusion length constant that provides the best fit.

Experimental data from ring 9 were compared to theoretical data calculated based on different diffusion length constants. Assumed values in the theoretical calculations include a 25μm $1/e^2$ Gaussian intensity profile diameter laser beam, gap width of 8μm, and total detector width obtained from visual inspection. Results showed that a diffusion length constant of 50μm±10μm (which falls within observed measurements [8]) gave the best fit between experimental and theoretical values. A plot of ring 9 normalized signal vs. distance is found in Fig. 6, and as can be seen from the graph the fit is quite good. As a test for the model, comparisons were made between experimental and measured results for many of the other rings and similar results were noted. Thus, it was concluded that a simple exponential function appears to adequately predict the gap response of the Insitec ring detector. The weighting function over the gap width can be written as:

$$w_{\theta edge} = \rho/\rho = e^{-x/xd} \qquad (4)$$

where $\rho(\theta)$ is the local responsivity, ρ is the maximum responsivity in the ideal active region of the detector, xd is the diffusion length constant, and x is the position measured from the ideal edge into the gap.

Now that the weighting function w_θ has been determined a new instrument matrix K can be calculated by substituting the measured gap weighting function of Eq. (4) into Eq. (3) in place of the usually assumed step function. To quantify the effect of the detector weighting function on the instrument matrix, two matrices were calculated; one assuming a step detector response, the other the actual measured gap response (and weighting values of 0 and 1 in the masked and idealized regions, respectively). A plot of the difference matrix (element by element) between the two matrices is presented in Fig. 7. The matrices were calculated on an area basis with rectangular weighting functions, uniform by volume within-class distributions, and a Fraunhofer diffraction approximation. The surface plot shows almost no change on the outer rings, while the difference increases as ring geometry decreases. This is expected, as the ratio of gap area to visual detector area is much greater for smaller rings than larger ones.

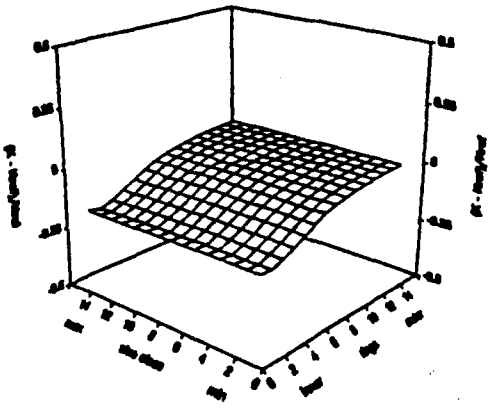

Fig. 7. Plot of the difference matrix between K based on a step response detector weighting function and K obtained with theoretical detector response weighting function (which accounts for detector response in the gap region between the mask and idealized detector boundary).

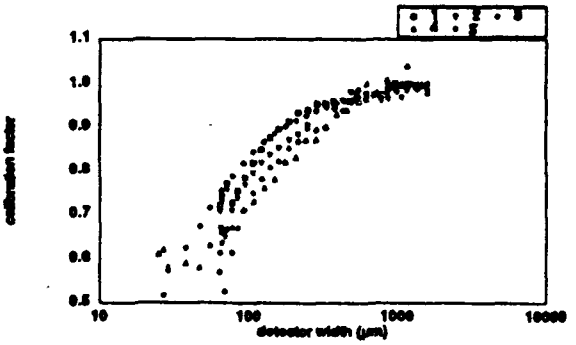

Fig. 8. Plot of calibration factors vs. detector width for various instruments and calibration techniques. The numbers in the legend correspond to the following: 1) Malvern 2600, instrument #1, uniform incoherent illumination [6,11]. 2) Malvern 2600, instrument #2, factory supplied calibration factors [9]. 3) Malvern 2600, instrument #3, uniform incoherent illumination [10]. 4) Insitec, uniform incoherent illumination. 5) Insitec, theoretical predictions based on gap response method.

It has already been mentioned that it is possible to predict calibration factors based on gap or transition region response as opposed to systematic between-detector variations in the responsivity. The accuracy of the "gap" calculated factors is based on the premise that the major contribution to calibration factors is from gap response. A predicted calibration factor is defined here as the ratio of the ideal detector output to the actual detector output when illuminated with light of uniform intensity. The ideal detector output is calculated by integrating the incident light intensity over the ideal, visual detector area while assuming that the weighting function w_θ is constant and equal to one. The actual detector output is found in the same manner except the area over which the integration is performed includes the gap region and the associated weighting function $w_{\theta edge}$. In equation form we have:

$$C_{pred} = \frac{\int I\,dA}{\int w_\theta\, I\,dA} = \frac{\int dA_{(ideal)}}{\int w_{\theta edge}\, dA_{(gap)} + \int dA_{(ideal)}} \qquad (5)$$

where C_{pred} is the predicted calibration factor and I is the intensity (W/m^2).

Traditionally, calibration factors have been determined based on illuminating the detectors with uniform light intensity. We determined two sets of calibration factors for the Insitec detector. One set of factors was calculated using Eq. (5), while the other set was determined using the uniform light method. Results of the two methods are displayed in Fig. 10 along with calibration factors from 3 different [9-11] Malvern 2600 instruments determined empirically with the uniform light method. Since the Insitec detector geometry differs slightly from the Malvern detector geometry, the calibration factors are plotted vs. detector width. As is seen from the plot the curves are in reasonable agreement. Noticed trends are that all factors decrease in value as detector area decreases. Consequently, the inner detectors over-respond relative to the outer detectors. Calibration factors determined from Eq. (5) are limited by the fact that experimental data were collected along two lines running through the center of the detector instead of scanning the entire detector surface. Additionally, in Eq. (5) it was assumed that the weighting function equals a constant over the ideal detector region, however, Fig. 4 shows slight variation in this region. One other area of uncertainty which we did not investigate is the ends of each detector. Though we accounted for the end region in the calculations the region is different from the rest of the perimeter regions in that a masked area is not found 8μm from the ideal detector boundary. A drawback to the uniform light method is that linear detector response is assumed with no cross-talk. If either of the above assumptions is not correct then errors in calibration factors will propagate through the remaining factors that need to be determined. This results from the requirement that values acquired from different light levels must be spliced together [3]. Overall, it appears that calibration factors calculated using Eq. (5) compare reasonably well with factors determined with the uniform light method, especially considering the fact that factors are for different detectors from different laboratories.

CONCLUSIONS

In conclusion, the transition region response has been measured and modeled for an Insitec detector. A simple exponential with a diffusion length constant of 50μm accurately predicted the experimental data. The detector weighting function has been calculated and incorporated into the instrument matrix K. Calibration factors for the Insitec detector have been predicted based on edge effects and were compared with calibration factors derived from the uniform light source technique. Both methods indicated that the inner rings over-respond relative to the outer, larger rings. It is difficult to conclude which method produces the more accurate results. The uniform light method has the disadvantage that detector signals resulting from several light levels must be measured and the calibration curves spliced together. The gap response model has the disadvantage that it is based on 2-dimensional results and it must be assumed that gap response is axisymmetric. Another independent technique for calculating calibration factors could help verify whether the gap or uniform light source is more accurate. The effect of using the theoretical calibration factors instead of the uniform light source factors would, in general, translate into slightly larger particle sizes because of the higher signals on the inner rings.

ACKNOWLEDGMENTS

This research was supported by the Air Force Office of Science Research, Air Force Systems Command, USAF, under grant AFOSR-90-0358, Dr. Julian Tishkoff, program manager. The U.S. government is authorized to reproduce and distribute reprints for governmental purposes notwithstanding any copyright notation thereon.

REFERENCES

1. E. D. Hirleman, "Particle Sizing by Optical, Nonimaging Techniques," in *Liquid Particle Size Measurement Techniques*, STP 848, J. M. Tishkoff, R. D. Ingebo, and J. B. Kennedy, Eds. (American Society of Testing Materials, Philadelphia, 1984), pp. 35-60.

2. J. Swithenbank, J. Beer, D. S. Taylor, D. Abbot, and C. G. McCreath, in *Experimental Diagnostics in Gas-Phase Combustion Systems*: AIAA Progress in Astronautics and Aeronautics, B. T. Zinn, ed., AIAA V. 23, pp. 421-447. (1977).

3. E. D. Hirleman, V. Oechsle, and N. A. Chigier, "Response Characteristics of Laser Diffraction Particle Size Analyzers: Optical Sample Volume Extent and Lens Effects," *Optical Engineering*, V. 23, No. 5, pp. 610-619 (1984).

4. M. Heuer, K. Leschonski, "Results Obtained with a New Instrument for the Measurement of Particle Size Distributions from Diffraction Patterns," Particle Characterization, V. 2 pp. 7-13 (1985).

5. E. D. Hirleman and L. G. Dodge, "Performance Comparison of Malvern Instruments Laser Diffraction Drop Size Analyzers," ICLASS Conference Proceedings, The Institute of Energy, London, V. 2, pp. IVA.3.1-IVA.3.6 (1985).

6. L. G. Dodge, "Calibration of the Malvern Particle Sizer," *Applied Optics*, V. 23, pp. 2415-2419 (1984).

7. E. D. Hirleman, "Uncertainties in Matrix Formulations of the Fraunhofer Diffraction Particle Size Problem," Proceedings of ILASS America Conference, Institute of Liquid Atomization and Spray Systems, pp. 1-5 (1989), Irvine, CA.

8. S. M. Sze, *Physics of Semiconductor Devices*, John Wiley and Sons, New York (1981).

9. G. S. Samuelsen, University of California, Irvine, CA (private communication).

10. E. A. Hovenac, NASA Lewis Research Center, Cleveland, Ohio (private communication).

11. L. G. Dodge, Southwest Research Institute, San Antonio, Texas (private communication).

a reprint from Applied Optics

General solution to the inverse near-forward-scattering particle-sizing problem in multiple-scattering environments: theory

E. Dan Hirleman

A general solution to the problem of measuring the size distribution of large particles in optically thick media by using small-angle light scattering is presented. The approach is general in the sense that no assumption of the form of the particle-size distribution function is required, although the particles must be distributed uniformly throughout the medium. The method is based on a successive order, discrete ordinates approach for modeling multiple-scattering phenomena and requires that the particle field be interrogated by using an array of near-forward input light angles. The scattering redistribution matrix is thereby determined, which permits a numerical inversion of the problem to obtain the single-scattering signature. Finally, conventional inverse scattering methods are used to reconstruct the particle-size distribution from the near-forward (single-scattering) light-scattering pattern.

Introduction

The phenomenon of multiple scattering significantly complicates the analysis of radiation transfer through particulate-laden media. Nonintrusive diagnostics for various flows depend on an understanding of light scattering and propagation and for this reason can unfortunately not be used in the many important systems and applications that involve optically thick media. We develop a general solution to the problem of measuring the size distribution of large particles in optically thick media using small-angle light scattering. Numerical experiments are used to demonstrate the feasibility of the technique.

In a previous paper by Hirleman[1] a theoretical approach to solving the direct problem (i.e., calculation of the scattering signature given the particle size distribution) for the case of near-forward scattering by particles that are large compared to the wavelength in optically thick media was presented. While other models exist for predicting the scattering properties of thick media, the discrete ordinates, successive order approach of this previous work[1] was developed specifically for incorporation into schemes for solving the inverse problem. We present a general solution for the corresponding inverse problem, i.e., that of estimating the size distribution function of an ensemble of large particles by using mathematical inversion of the near-forward-optical-scattering properties of the optically thick medium.

Theory

Consider a particle-laden medium illuminated by a planar electromagnetic wave at an arbitrary (but small) angle Θ_{inc} relative to the laboratory optical Z axis. The coordinate system of interest is shown in Fig. 1 with a single particle at the origin and for a wave incident at $\Phi_{inc} = 0$. Assume that the scattering phenomenon is axisymmetric, i.e., with no azimuthal Φ dependence of the scattered field as would be the case for an effectively infinite medium of spherical particles. If the incident field actually consisted of the superposition of waves covering all possible values of Φ_{inc} for a given Θ_{inc} (i.e., a hollow cone of incident light), the overall scattering characteristics of the medium would be symmetric about the optical axis. If nonspherical particles were present, so that the individual scattering signatures were not axisymmetric, the overall radiation transfer problem could still be considered axisymmetric if there were a large number of randomly oriented particles in the medium. It is also assumed that the scattering processes involved are linear (in the sense of a linear system). The linear system assumption requires that, if the incident optical power is multiplied by a constant, the scattered energy leaving the medium in all directions is

The author is with the Department of Mechanical and Aerospace Engineering, Arizona State University, Tempe, Arizona 85287-6106.

Received 5 July 1990.
0003-6935/91/334832-07$05.00/0.

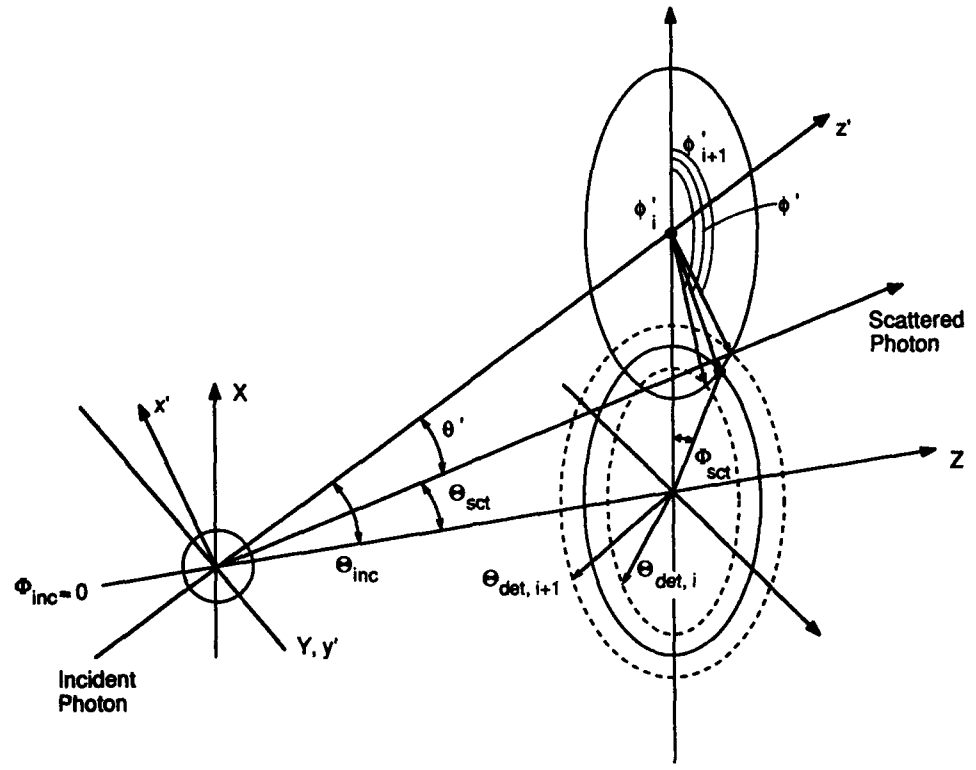

Fig. 1. System for analysis of multiple scattering. The incident electromagnetic energy is shown as a photon passing through the origin of the laboratory *XYZ* coordinate system traveling in a direction defined by angles Φ_{inc} and Θ_{inc}. A plane wave traveling in the same direction would be scattered by the spherical particle shown at the origin in a scattering pattern axisymmetric with respect to the Poynting vector, i.e., axisymmetric about the z' axis. The scattered light, indicated as a scattered photon in the figure, is transformed back into the laboratory coordinate system before analysis of the next scattering event.

similarly multiplied by the same factor. Finally, dependent scattering is neglected; i.e., it is assumed that scattered fields add incoherently (on an intensity rather than amplitude basis). It is important to note here that the total scattered energy that leaves the medium in any direction is not necessarily proportional to the number of particles in the system; i.e., the energy scattered in a given direction by an M-particle medium is not equal to M times the scattering contribution of one isolated particle in conditions of significant multiple scattering. However, the classical definition of a linear system involves proportionality between input and output variables (in this case the incident and scattered energy) but does not constrain the effects of changing, say, the extent or population density of the medium.

The approach used here is based on discretizing the range of incident and scattering angles into a finite number of directions, each representing a finite range of scattering angles. This term discrete ordinates has been used by van de Hulst[2] and others to describe this general method. For the axisymmetric problem of interest here the discrete scattering-angle ranges are independent of the azimuthal scattering angle Φ and subtend 2π rad in Φ for discrete values of Θ. These discrete values of incident and scattering cones represented by Θ are then the discrete ordinates of the system. We define[1] a scattering vector $\mathbf{S}$ so that the ith element of $\mathbf{S}$ contains a measure of the radiant energy proceeding in directions represented by the angle Θ_i. The effect of a scattering medium then is to operate on the incident light and redistribute the radiant energy over the various Θ_i. (Some of the light may also be absorbed in the medium, and this effect is considered below.) It is convenient to define a scattering redistribution matrix $\mathbf{H}_m$ so that the matrix element in the ith row and the jth column $\mathbf{H}_m(i, j)$ is the gain or efficiency with which optical energy incident in a direction represented by Θ_j is redistributed by the medium into direction Θ_i. The effect of the linear medium can be written as

$$\mathbf{S}_m = \mathbf{H}_m \mathbf{S}_{inc}, \tag{1}$$

where $\mathbf{S}_{inc}$ is a vector so that the jth element represents the optical energy incident on the medium in direction Θ_j and $\mathbf{S}_m$ is a vector so that the ith element represents the amount of optical energy exiting the medium in direction Θ_i. Note that $\mathbf{S}_{inc}$ and $\mathbf{S}_m$ are somewhat analogous to the Stokes vectors from the electromagnetic scattering theory,[2] except that polarization is not considered. The assumption that polarization effects are negligible is reasonable for the near-forward-scattering regime of interest here. The subscripts m on $\mathbf{H}_m$ and $\mathbf{S}_m$ indicate that these apply to the general multiple-scattering situation, i.e., $\mathbf{H}_m$ represents the redistribution effect of a general medium and $\mathbf{S}_m$ is the scattering signature that may

include multiple-scattering effects. These are distinct from a single-scattering redistribution matrix $\mathbf{H}$, and scattering-order vectors $\mathbf{S}_n$ are defined below. $\mathbf{H}_m$ is a function of the particle-size distribution and the optical depth of the medium.

Selection of the appropriate number of and the specific values of the discrete scattering angles Θ_i (i.e., the discrete ordinates) depends on the scattering properties of the medium. The number of angles considered is an important factor that controls the accuracy with which the discrete approximation in Eq. (1) approximates the actual radiation transfer process that is actually continuous in Θ and Φ. We select Θ_i to be consistent with the photodetector geometries used in our experimental work on particle sizing. It has been shown by Hirleman[3] that the optimal detector geometry for particle sizing in the large-particle, small-scattering angle regime (where Fraunhofer diffraction theory is valid) consists of log-scaled rings. In the theoretical work reported here we use collection aperture geometries corresponding to the ring elements of the RSI ring/wedge detector[4] for which dimensional data are available.[5] We consider optical energy proceeding nominally along the optical axis as the first element of $\mathbf{S}_{inc}$ and $\mathbf{S}_m$, so that this element, defined by the representative angle Θ_0, subtends a range of scattering angles from zero to a small angle corresponding to the central, circular detector element used for measuring extinction. The angle range considered, *i.e.*, $\Theta_0 \rightarrow \Theta_n$, where $n + 1$ is the number of discrete ordinates, must be sufficiently large that only a negligible amount of optical energy falls outside it. For that reason the value of Θ_n required for a particular problem depends on the scattering properties of the medium (i.e., through the particle-size distribution) and the optical depth of the medium.

The conventional method for particle sizing by using near-forward light-scattering signatures involves[1,3,5] interrogation of the medium with a collimated input beam that defines an optical axis ($\Theta = 0$) that is centered in the ring detector. In this case the normalized incident energy vector $\mathbf{S}_{inc}$ is given by

$$\mathbf{S}_{inc} = [1, 0, 0, \ldots 0]^T. \quad (2)$$

Now from Eq. (1) we see that in the conventional system, with the angular distribution of the incident optical energy given by Eq. (2), the output scattering signature $\mathbf{S}_m$ is just equal to the first column of $\mathbf{H}_m$. The direct problem, i.e., calculation of the output scattering signature given an input beam and a medium defined by the particle-size distribution and an optical depth b, can be viewed as determining $\mathbf{H}_m$ and using Eq. (1) to predict $\mathbf{S}_m$. The inverse-scattering particle-sizing problem is then a matter of determining a particle-size distribution, which in theory should have produced the observed scattering signature $\mathbf{S}_m$. To do this it is in turn necessary to be able to calculate theoretically the matrix $\mathbf{H}_m$ valid for an arbitrary particle-size distribution and optical depth.

If it is desired to extract n unique pieces of information about the particle-size distribution in the medium, it is necessary to make at least n measurements. Often the n pieces of information (unknowns) are the quantity of particles in n discrete size classes, and the measurements of the light scattered at n discrete angles provides n equations to produce an $n \times n$ linear system. Now interrogation of a medium with an incident field as indicated by Eq. (2) resulted in an experiment that produced n measurements, i.e., the elements of $\mathbf{S}_m$. Further consideration reveals that Eq. (1) can in fact support n independent experiments, each consisting of scattering measurements at n angles (i.e., n^2 total independent measurements). Any of these experiments could be used to obtain an estimate of the particle-size distribution function, although conventional near-forward-scattering methods use only one. An $\mathbf{S}_{inc}$ vector with the jth element as the only nonzero element represents a hollow cone of illumination with half-angle Θ_j. For an experiment of this type only the jth column of $\mathbf{H}_m$ would enter the problem. An optical system designed to produce hollow-cone illumination as discussed is shown in Fig. 2. A programmable mask with an array of n annular shutters is placed in the front focal plane of a transmitting lens. This ring or cylinder of light transmitted through the mask is transformed by the lens to contain only a small range of angles in the back focal plane of the lens; i.e., a hollow cone with half-angle Θ, where Θ is related to the mean radius r of the annular shutter and the lens focal length f by $\Theta = r/f$. A matched annular shutter array is used at

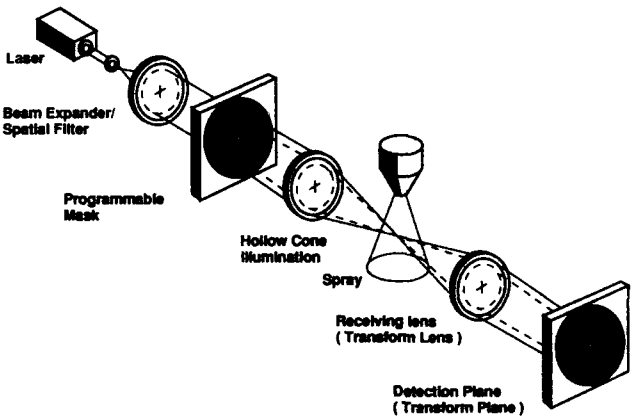

Fig. 2. Simplified schematic of an optical system that allows multiangle interrogation and multiangle scattering measurements of a spray or particle field. A programmable annular shutter or mask in the front focal plane of the transmission lens creates an annular ring or cylinder of light. This is then converted into a hollow cone of light (all light traveling with nominally the same angle Θ_{inc} relative to the optical axis) by the Fourier transform process of the lens. Light scattered by the medium is transformed from an angular to a spatial pattern at the back focal plane of the receiving lens. Light scattered into discrete ranges of ϕ and Θ are sampled by another annular shutter array at the detector plane and transmitted to a detector (not shown) behind the shutter array.

the back focal plane of the receiving lens, and for each incident cone angle the system is cycled through all rings at the detector plane.[6]

Theory for Determination of $\mathbf{H}_m$

It has been pointed out that Eq. (1) can theoretically be used to determine particle-size distributions in arbitrary media, if we assume that the elements of $\mathbf{H}_m$ can be theoretically expressed as a function of the quantity of particles in n discrete size classes. However, the stability of the proposed inverse solution is in question, and methods for calculating $\mathbf{H}_m$ are not in the literature. In this section a derivation of $\mathbf{H}_m$ is presented.

Recall that $\mathbf{H}_m$ is defined so that the element (i, j) is related to the probability that light incident at Θ_j will leave the medium in a direction specified by Θ_i. This probability in turn depends on the single-scattering phase function and the extent of the medium. If the medium is optically thin, multiple scattering can be neglected and the problem is relatively simple as the phase function can be used directly. The successive orders approach used here[1] effectively reduces the problem to an analysis of a sequence of single-scattering events, each of which is easily modeled. It is in this context that the single-scattering redistribution matrix $\mathbf{H}$ is defined so that H_{ij} represents the probability that a photon incident on a medium at an angle representative of the jth detector will leave the *next* scattering event in a direction corresponding to the ith detector. Note that $\mathbf{H}$ depends on the detector geometry and the scattering characteristics of the medium, which is a function of the unknown particle-size distribution but not on the optical depth or extent of the medium. The matrix $\mathbf{H}$ is needed for use in a recursive scattering-order equation:

$$\mathbf{S}_n = \mathbf{H}\mathbf{S}_{n-1}, \tag{3}$$

where $\mathbf{S}_{n-1}$ and $\mathbf{S}_n$ are the scattering signature vectors of light (photons) scattered exactly $n - 1$ and n times, respectively. A special case of Eq. (3) is for unscattered (incident) energy:

$$\mathbf{S}_1 = \mathbf{H}\mathbf{S}_{\text{inc}} = \mathbf{H}\mathbf{S}_0. \tag{4}$$

Inspection of Eq. (4) indicates that the first column of $\mathbf{H}$ is just the normalized scattering signature, which would be obtained from an optically thin aerosol illuminated with a collimated beam. Now $\mathbf{H}$ is theoretically determined (for a given size distribution) by using an analysis that combines some transformations that relate light-scattering and laboratory coordinate systems with the calculation of scattering phase functions. The development[1] requires a small-angle approximation and therefore may be considered to be valid for relatively large particles. The small-angle assumption simplifies calculation of the probability distribution over the number of scattering events that are related to the physical (as opposed to optical) medium width through the optical depth b. Now the composite scattering signature $\mathbf{S}_m$ (superposition over all scattering orders $\mathbf{S}_{0\ldots n}$) is given by[1]

$$\mathbf{S}_m = \exp(-b)[\mathbf{I} + a_f b\mathbf{H} + (a_f b)^2/2\mathbf{H}^2 + (a_f b)^3/6\mathbf{H}^3 + \cdots]\mathbf{S}_{\text{inc}}, \tag{5}$$

where $\mathbf{I}$ is the identity matrix and a_f is defined as a forward-scattering albedo where $a_f = 0.5$ in the diffraction regime of interest here.

Using the definition for the logarithm of a matrix in combination with Eq. (5) we obtain

$$\mathbf{S}_m = \exp(-b)\exp(a_f b\mathbf{H})\mathbf{S}_{\text{inc}}, \tag{6}$$

and by comparing Eqs. (1) and (6) we obtain

$$\mathbf{H}_m = \exp(-b)\exp(a_f b\mathbf{H}), \tag{7}$$

which provides a rather straightforward link between the single-scattering redistribution matrix $\mathbf{H}$ and the general medium matrix $\mathbf{H}_m$. Use of the optical system of Fig. 2 permits measurement of the n^2 elements of $\mathbf{H}_m$ according to Eq. (1). Inverting Eq. (7) we obtain

$$\mathbf{H} = \ln[\exp(b)\mathbf{H}_m]/(a_f b) \tag{8}$$

which provides a link back to $\mathbf{H}$ if $\mathbf{H}_m$ and b are measured experimentally. Recall that the first column of $\mathbf{H}$ is just the single-scattering signature, which would be obtained from collimated illumination of an optically thin medium. Conventional near-forward-scattering instruments routinely use this single-scattering signature for $\Theta_{\text{inc}} = 0$ in an inversion process to obtain the particle-size distribution. Therefore, if the first column of $\mathbf{H}$ can be determined, conventional single-scattering inversion schemes can be applied. The mathematical procedure given in Eq. (8) whereby operations are performed on an experimentally measured $\mathbf{H}_m$ is, in a sense, equivalent to reaching into the medium to collect photons that have been scattered once and only once.

Relationship to the Inverse Single-Scattering Problem

The single-scattering inverse problem is generally written[3] in a form

$$\mathbf{S} = \mathbf{K} \cdot \mathbf{N}, \tag{9}$$

where $\mathbf{S}$ is the scattering signature over the detectors, $\mathbf{N}$ is the unknown size distribution vector so that $\mathbf{N}_j$ represents the quantity of particles in the jth size class, and $\mathbf{K}$ is the scattering matrix so that element K_{ij} indicates the amount of energy that a unit quantity of particles representative of the jth size class would scatter into the ith detector assuming single scattering. Now the elements of $\mathbf{K}$ can be determined by using the Lorenz–Mie scattering theory or some approximation such as the Fraunhofer diffraction theory. The matrix is calculated by using weighting functions for both the size classes and the detector geometries.[3]

Now it would be useful to formulate the inverse

multiple-scattering problem as a linear system of the form:

$$\mathbf{S}_m = \mathbf{K}_m\mathbf{N}, \tag{10}$$

where we must define (and determine) $\mathbf{K}_m$ as the scattering coefficient matrix that applies for a multiple-scattering medium. The inverse multiple-scattering problem would then involve inversion of the matrix $\mathbf{K}_m$ or, in the case of an ill-conditioned $\mathbf{K}_m$, some other method for solving the linear system given by Eq. (10) would be used. Now it has previously been noted that the matrix $\mathbf{H}$ depends on the particle-size distribution through its effect on the scattering signature, so we choose to define a different $\mathbf{H}$ for each size class of $\mathbf{N}$. If we denote ${}_j\mathbf{H}$ as the single-scattering redistribution matrix for particles representative of the jth size class and ${}_j\mathbf{H}_m$ as the multiple-scattering redistribution matrix for a medium containing only particles in size class j, Eq. (1) becomes for this case

$${}_j\mathbf{S}_m = {}_j\mathbf{H}_m\mathbf{S}_{\text{inc}}\mathbf{N}_j, \tag{11}$$

where ${}_j\mathbf{S}_m$ is the multiple-scattering signature produced by a quantity $\mathbf{N}_j$ particles from size class j with illumination specified by $\mathbf{S}_{\text{inc}}$ and where the multiplication by the scalar N_j is a scalar product but the ${}_j\mathbf{H}_m\mathbf{S}_{\text{inc}}$ product is a vector operation. When we expand Eq. (11), using the definition in Eq. (7), we obtain:

$${}_j\mathbf{S}_m = \exp(-b_j)\exp({}_j\mathbf{H}a_jb_j)\mathbf{S}_{\text{inc}}\mathbf{N}_j, \tag{12}$$

where ${}_j\mathbf{H}$ is defined as the single-scattering redistribution matrix in a medium containing only particles representative of the jth size class and b_j in Eq. (12) is defined by

$$b_j \equiv \rho_j C_{\text{ext},j}\ell = (N_j/V)C_{\text{ext},j}\ell, \tag{13}$$

where ρ_j and $C_{\text{ext},j}$ are the number density (number per unit volume) and mean extinction cross section, respectively, of particles in size class j, ℓ is the physical length of the medium, and V is the volume within which the number quantity N_j applies. Note that taking the particle number density $\rho_j = (N_j/V)$ requires that N_j be defined on a number basis (as opposed to an area or volume basis). The quantities ρ_j and $C_{\text{ext},j}$ would be obtained by integrating over the size range of the jth size class by using an appropriate within-class weighting function.[3]

To return to a form such as in Eq. 1 it is tempting to use a superimposition of the scattering signatures for the j size classes from Eq. (12). It is the case for which the composite-scattering signature could be calculated as a linear combination of signatures from each class, but unfortunately the correct scattering signatures to be used in the summation are not given by Eq. (12). Equation (12) applies to a medium containing only one size and does not apply in the general case with particles from a multiplicity of size classes. This nonlinearity or coupling of the equations would come through the fact that the redistribution matrix for a given size class in a polydisperse medium depends on the populations of all the other size classes. In other words the matrix $\mathbf{K}_m$ in Eq. (10) cannot be calculated independent of a knowledge of the particle-size distribution $\mathbf{N}$, and hence Eq. (10) is not a linear system in the conventional sense. However, the matrix $\mathbf{K}_m$ could be calculated for a given $\mathbf{N}$, and the predicted scattering signature $\mathbf{S}$ from Eq. (10) could be compared with a measured one to provide the basis for an iterative solution to determine a best fit $\mathbf{N}$. In contrast the approach suggested here is different. The rather involved calculations that are required to account for a coupling of the multiple scattering between size classes are replaced here by a number of independent measurements that serve to determine this coupling experimentally. The results of numerical studies of the performance of the new approach are discussed below.

Results of Numerical Experiments

To determine the feasibility of the proposed approach numerical experiments were performed to simulate the process of (1) measuring b and $\mathbf{H}_m$ by using multiangle interrogation, (2) calculating an estimate of the single-scattering redistribution matrix $\mathbf{H}$ by using Eq. (8), and finally (3) reconstructing a particle-size distribution function by inverting Eq. (9). To calculate $\mathbf{H}_m$ it is first necessary to obtain a theoretical $\mathbf{H}$ to use in Eq. (7). A plot of the calculated matrix $\mathbf{H}$ for National Bureau of Standards SRM 1003a using the RSI detector geometry within an optical system with a receiving (transform) lens focal length of 125 mm is given in Fig. 3. Note that the axis in the

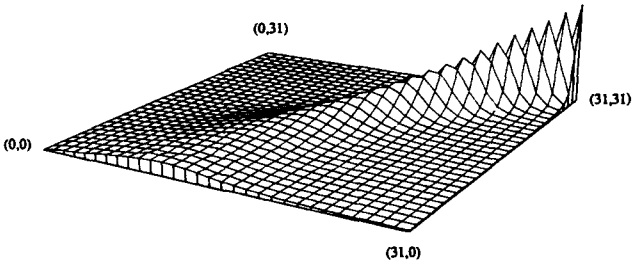

Fig. 3. Plot showing the calculated single-scattering redistribution matrix $\mathbf{H}$. The redistribution matrix $\mathbf{H}$ was calculated for the particle-size distribution of National Bureau of Standards (U.S.) SRM 1003A for a laser diffraction system that uses the RSI detector geometry[4,5] with a transform lens focal length of 125 mm and the successive order, discrete ordinates multiple-scattering model.[1] The upper left element of $\mathbf{H}$, i.e., H_{00} or $H(0, 0)$, is shown on the left and applies to light incident at the smallest angle Θ_0 ($\Theta_0 \approx 0$ or collimated input), which is scattered back into the same angle (identically forward scattering) by the next scattering event. The lower point in the foreground $H(0, 31)$ represents collimated incident light, which is scattered into the 31st ring detector, and the axis in the left foreground is the single-scattering signature for a conventional diffraction system (collimated input scattered over 31 rings). The ridge at the right of the figure culminating at $H(31, 31)$ is caused by the fact that the outer RSI ring detectors are much larger than the inner ones.[5]

foreground, lower left, corresponds to the first column of **H**, i.e., the single-scattering signature that would be obtained with collimated ($\Theta_{inc} = 0$) incident radiation as given by Eq. (2). For $f = 125$ mm and Natl. Bur. Stand. (U.S.) SRM 1003a, the peak signal occurs in the region of ring detectors 10 and 11. The upper left element H (0, 0) corresponds to light incident at $\Theta = 0$, which is literally forward scattered so that $\theta_{act} = 0$. As one moves through columns of **H** (i.e., moving toward the upper right background) the matrix row at which the scattering maximum occurs shifts toward the outer detectors (larger i for H_{ij}). Finally at $H(31, 31)$ most of the energy incident at an angle corresponding to the large 31st ring of the RSI detector is rescattered into the same detector. Plots of $\mathbf{H}_m$ matrices calculated made by using Eq. (7) for the same particle-size distribution and optical system but at several optical depths are shown in Fig. 4. The **H** and $\mathbf{H}_m$ matrices are identical in the limit of small optical depth b, and the similarities are seen by comparing Figs. 3 and 4(a). However, as b increases the first columns of $\mathbf{H}_m$ (foreground) indicate the scattering signatures that would be obtained for collimated incident radiation as given by Eq. (2). The shift of the scattered energy toward larger angles (lower rows of the matrices) characteristic of multiple scattering is apparent in the progression through Figs. 4(a)–4(c). That this shift toward larger angles resembles small particles to a conventional near-forward-scattering instrument has been well documented.[7,8]

The inverse scattering scheme proposed here requires measurement of the matrix $\mathbf{H}_m$ and the optical depth b and the numerical determination of **H** with Eq. (8). For this work we first calculated **H** and then $\mathbf{H}_m$ as shown in Figs. 3 and 4. A simulation of the experimental measurement of $\mathbf{H}_m$ was then made by perturbing the calculated elements of $\mathbf{H}_m$ with a Gaussian random number generator. The random noise added was multiplicative and was specified whereby the standard deviation of the Gaussian random noise was a fraction of the signal on each detector.

Another experimental difficulty will be measurement of the diagonal elements of $\mathbf{H}_m$, which represent light scattered into the same detector aperture as the incident radiation. Since the scattering is often an order of magnitude or more smaller than the unscattered (transmitted) energy, the elements will be difficult to measure accurately. In the simulation of the experiment the diagonal elements were determined by averaging the adjacent off-diagonal elements. Implicit in this procedure is that optical and electronic cross talk between detector apertures is negligible.

After the $\mathbf{H}_m$ matrix was perturbed to simulate an experimental measurement the inversion indicated by Eq. (8) was performed. The results are presented

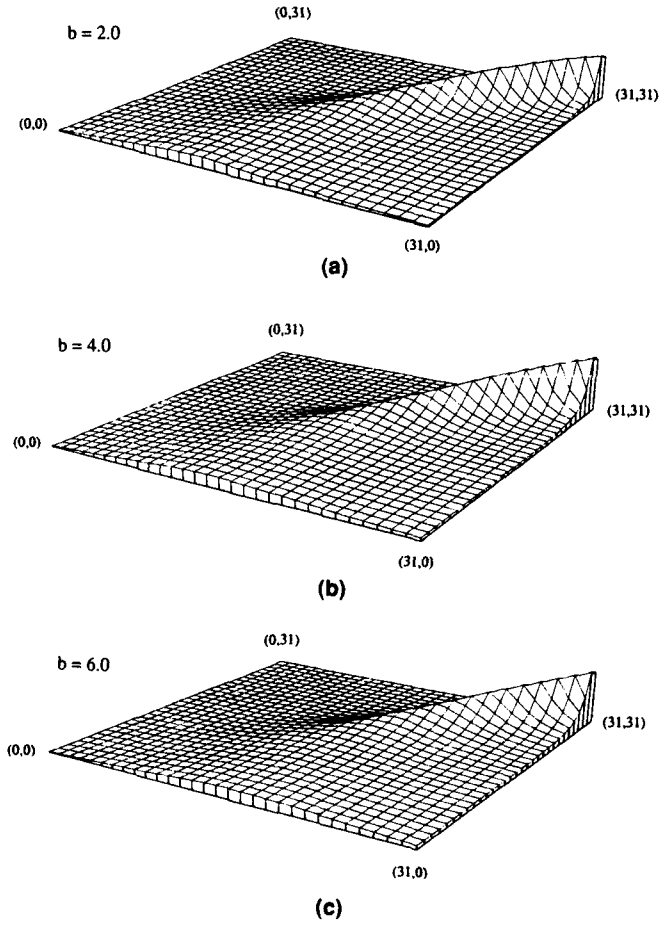

Fig. 4. Calculated multiple-scattering redistribution matrix $\mathbf{H}_m$. The redistribution matrix $\mathbf{H}_m$ was calculated for the particle-size distribution of National Bureau of Standards (U.S.) SRM 1003A for a laser diffraction system that uses using the RSI detector geometry[4,5] with a transform lens focal length of 125 mm and the successive order, discrete ordinates multiple-scattering model.[1] The plots correspond to three different values of the optical depth b as indicated. The upper left element of $\mathbf{H}_m$, i.e., $H_m(0, 0)$, is shown on the left and applies to light incident at the smallest angle Θ_0 ($\Theta_0 \approx 0$ or collimated input), which is scattered back into the same angle (identically forward scattering) after passing through the entire medium. The lower point in the foreground of the figure $H_m(0, 31)$ represents collimated incident light, which is scattered into the 31st ring detector, and the axis in the left foreground shows the scattering signature that would be obtained by a conventional diffraction system (collimated input scattered over 31 rings). The progression through increasing values of b shows the expected shift of scattered light to larger angles.

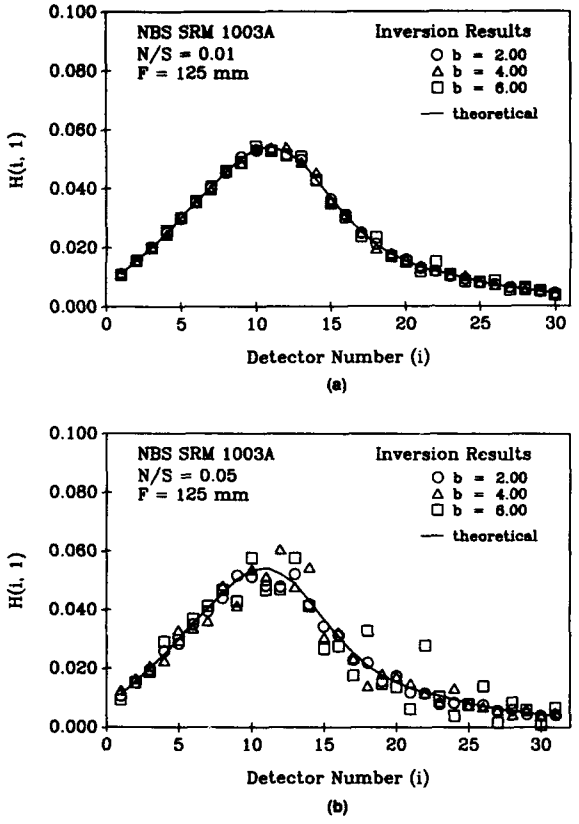

Fig. 5. First columns of the single-scattering redistribution matrix **H** reconstructed in numerical experiments by using an inversion of synthetic scattering data given by Eq. (8). The assumed optical system had an RSI ring detector[5] with f = 125-mm transform lens, and the particle-size distribution assumed was National Bureau of Standards (U.S.) SRM 1003a. The calculated elements of the $\mathbf{H}_m$ matrix (shown in Fig. 4) were perturbed with two different levels of simulated Gaussian (multiplicative) noise with standard deviations of (a) 1% and (b) 5%.

in Fig. 5, which shows the first column of **H** as obtained from Eq. (8). To review, the first column of **H** is an estimate of the single-scattering signature, which would be obtained by using collimated on-axis incident radiation. In conventional particle-sizing methods using near-forward scattering it is the first column of **H** that is hopefully measured by the detectors. For that reason, then, inversion schemes used in conventional methods for optically thin aerosols can be used on the first column of the reconstructed **H** matrix to obtain the particle-size distribution. The various schemes for performing the inverse single-scattering problem are discussed elsewhere.[3,9]

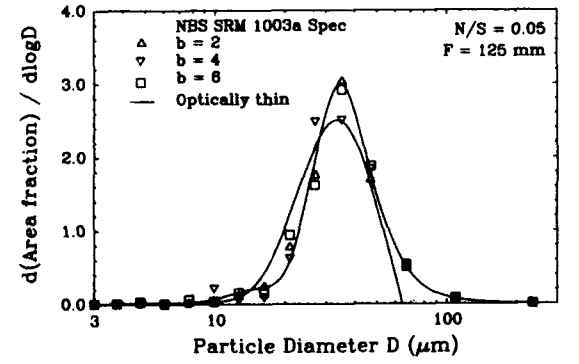

Fig. 6. Results of the numerical inversion of the scattering signatures of Fig. 5 Reconstructed particle-size distributions are shown. The size distributions were obtained by solving[9] Eq. (9), where the scattering signature **S** was taken as the first column of the reconstructed **H** matrices as shown in Fig. 5.

The performance of the proposed method based on the numerical studies is demonstrated in Fig. 6. Here the actual and reconstructed size distributions for SRM 1003a are shown for several optical depths and for 5% simulated Gaussian random noise. Reasonable reconstructions of the particle-size distribution are feasible up to $b = 6$ for the conditions studied here.

Conclusions

A scheme for solving the inverse scattering problem in optically thick media has been presented. Numerical experiments indicate that the method is feasible for reconstructing particle-size distributions in realistic measurement conditions.

This research was supported by the Air Force Office of Science Research, Air Force Systems Command, U.S. Air Force, under grant AFOSR-84-0187, Julian Tishkoff, program manager. The U.S. government is authorized to reproduce and distribute reprints for governmental purposes notwithstanding any copyright notation thereon.

References

1. E. D. Hirleman, "Modeling of multiple scattering effects in Fraunhofer diffraction particle size analysis," Part. Charact. **5**, 57–65 (1988).
2. H. C. van de Hulst, *Multiple Scattering* (Academic, New York, 1980).
3. E. D. Hirleman, "Optimal scaling for Fraunhofer diffraction particle sizing instruments," Part. Charact. **4**, 128–133 (1988).
4. Recognition Systems, Inc., Van Nuys, Calif., no longer in business. More recently available from ARC, Inc., Rochester, N.Y. The detector is covered in N. George, J. Thomasson, and A. Spindel. "Photodetector for real-time pattern recognition," U.S. Patent 3,689,772 (5 September 1970).
5. E. D. Hirleman, "Particle sizing by optical, nonimaging techniques," in *Liquid Particle Size Measurement Techniques*, STP 848, J. M. Tishkoff, R. D. Ingebo, and J. B. Kennedy, eds. (American Society of Testing Materials, Philadelphia, Pa., 1984), pp. 35–60.
6. E. D. Hirleman and P. A. Dellenback, "Faraday-effect light valve arrays for adaptive optical instruments," in *Optical Methods in Flow and Particle Diagnostics*, W. H. Stevenson, ed. (Laser Institute of America, Toledo, Ohio, 1988), Vol. 63, pp. 6–11.
7. L. G. Dodge, "Change of calibration of diffraction-based particle sizers in dense sprays," Opt. Eng. **23**, 626–630 (1984).
8. P. G. Felton, A. A. Hamidi, and A. K. Aigal, "Measurement of drop size distribution in dense sprays by laser diffraction," Report 431 HIC, Department of Chemical Engineering, University of Sheffield, U.K. (1984); in *Proceedings of the Third International Conference on Liquid Atomization and Spray Systems* (Institute of Energy, London, 1985).
9. J. H. Koo, "Particle size analysis using integral transform techniques on Fraunhofer diffraction patterns," Ph.D. dissertation (George Washington University, Washington, D.C., and Arizona State University, Tempe, Ariz., 1987).

From Proceedings of the 2nd International Congress on Optical Particle Sizing, March 5-8, 1990, Tempe, AZ.

PARTICLE SIZING ERRORS ASSOCIATED WITH THE FRAUNHOFER DIFFRACTION ASSUMPTION IN THE ANOMALOUS DIFFRACTION REGIME

S. B. Kenney and E. Dan Hirleman
Mechanical and Aerospace Engineering Department
Arizona State University
Tempe AZ 85287-6106

INTRODUCTION

The optical measurement technique commonly known as the Fraunhofer diffraction particle sizing method involves measuring the near forward scattering signature of an ensemble of large particles followed by a mathematical inversion procedure to determine the particle size distribution function. Of interest in this paper are errors introduced by a lack of knowledge of the particle relative refractive index. The near-forward scattering signature of an ensemble of particles will change as the refractive index of the particles approaches that of the surrounding medium. Under these conditions (and using a geometric optics model) the refracted light is increasingly directed into near-forward angles, interfering with the diffracted light, and thereby altering the near-forward scattering pattern. A particle sizing instrument based entirely on Fraunhofer diffraction formulas will give erroneous results when the refractive index of the particles is similar to that of the surrounding medium. It is these changes in the near forward scattering signature as the refractive indices change, and their effects on the size distribution which would be measured by such a particle sizing instrument, which are considered in this paper.

MATHEMATICAL FORMULATION

The most general equation governing Fraunhofer diffraction particle sizing is a Fredholm integral equation of first order and first kind and can be formulated as:

$$i(\theta) = I_{inc}/k^2 \int_0^\infty k_b(\alpha,\theta)\, n_b(\alpha)\, d\alpha \tag{1}$$

where: $i(\theta)$ is the intensity (W/sr) diffracted at near-forward scattering angles θ; I_{inc} is the irradiance (W/m^2) incident on the particles (assumed constant); k is the wavenumber $2\pi/\lambda$; λ is the wavelength; α is the size parameter $\pi D/\lambda$ where D is the particle diameter; $n_b(\alpha) = n(\alpha)\alpha^b$ where $n(\alpha)d\alpha$ is number of particles in the laser beam with sizes between α and $\alpha + d\alpha$ (n is an unnormalized probability density); b is a scaling parameter determined by the instrument designer which represents the measure of the quantity of particles used as the solution basis (e.g. for number, area, or volume bases the parameter b would equal 0, 2, or 3 respectively); and $k_b(\alpha,\theta)$ is a general scattering function which gives the scattering contribution of a unit quantity of particles of size α into angle θ. Particle sizing using Eq. (1) requires measurement of $i(\theta)$ followed by determining the $n_b(\alpha)$ which would produce a calculated $i(\theta)$ signature (using Eq. (1)) which best fits in some sense the measured $i(\theta)$. Clearly, the function $k_b(\alpha,\theta)$ must be known to use Eq. (1) in the inversion process, and full Lorenz-Mie expressions or approximations such as Fraunhofer diffraction theory may be used.

Equation (1) represents an infinite set of equations (one for each value of θ) in an infinite set of unknowns ($n_b(\alpha)$ for all possible α). In practice, however, it is impossible to make an infinite number of measurements of the scattered light distribution, and therefore a finite number of measurements at a set of discrete angles is usually made. By discretizing the equations we obtain a system of m_θ equations in m_α unknowns where m_θ is the number of discrete detectors and m_α is the number of discrete size classes. We write the linear system as:

$$\mathbf{I} = \mathbf{K} \cdot \mathbf{N} \tag{2}$$

In Eq. (2) the m_θ elements of the vector I represent the measured scattering signature; the m_α elements of N contain the bth partial moments of the number of particles in the size class; and K is the instrument matrix whereby element K_{ij} represents the diffraction contribution of a unit measure of particles in the jth size class onto the ith detector. The elements of K are:

$$K_{ij} = \int_0^\infty k_b(\alpha,\theta_i)\, w_\alpha(\alpha,\alpha_j)\, w_\theta(\theta,\theta_i)\, d\alpha\, d\theta \tag{3}$$

where $w_\alpha(\alpha,\alpha_j)$ is a weighting function for the jth size class and $w_\theta(\theta,\theta_i)$ is a weighting function describing the sampling process of the detector apertures. Now the solution or measured particle size distribution indicated by N in Eq. (2) can in theory be obtained by inverting the matrix K.

When the refractive index of the medium approaches that of the particles, the assumptions inherent in a kernal based on Fraunhofer diffraction are no longer valid. Calculations of near forward scattering signatures in this case are based on theory presented by van de Hulst [1957] where the term *anomalous diffraction* was coined to describe the condition when α is large and the refractive index denoted m approaches that of the surrounding medium. A parameter ρ is defined as:

$$\rho = 2\alpha\,|m-1| \tag{4}$$

which physically represents the phase lag suffered by a ray that passes through a sphere along a full diameter relative to a ray which passed undisturbed through the surrounding medium. The presence of the sphere does not alter the amplitude of the field at some position beyond the sphere, but rather affects only the phase. The phase lag can be calculated at some plane past the sphere and a direct application of Huygen's principle gives both the extinction and scattering diagrams. The intensity distribution is found by calculating the amplitude function $A(\rho,z)$ where $z = \alpha\theta$. An angle τ is defined as the

angle between the perpendicular bisector of the incident ray and the radius of the particle drawn from the incident point of the ray on the sphere. The amplitude function is given by:

$$A(\rho,z) = \int_0^{\pi/2} (1-e^{-i\rho\sin\tau}) J_0(z\cos\tau) \cos\tau \sin\tau \, d\tau \tag{5}$$

which is derived by applying Huygen's principle to a plane just beyond the sphere. The following expansion of the integral assumes that m is real and the absorption coefficient equals zero. The real and imaginary parts of the integral $A(\rho,z)$ are evaluated separately. If the substitution $\gamma = (\pi/2)-\tau$ is made, the imaginary part of the integral is transformed to Sonine's second integral and is represented by:

$$\mathrm{Im}A = (\rho/y^2)(\pi y/2)^{1/2} J_{3/2}(y), \qquad \text{where } y^2 = \rho^2 + z^2 \tag{6}$$

The real part is expressed as series expansions. Two different expansions are necessary for small and large values of ρ. For small ρ the first series expansion is:

$$\mathrm{Re}A = \rho^2(1/z^2)J_2(z) - (\rho^4/1*3)(1/z^3)J_3(z) + (\rho^6/1*3*5)(1/z^4)J_4(z) + \ldots \tag{7}$$

The expansion for large values of ρ is given by:

$$\mathrm{Re}A = (1/z)J_1(z) + (\rho/y^2)(\pi y/2)^{1/2}Y_{3/2}(y) + (1/\rho^2)J_0(z) + (1*3/\rho^4)zJ_1(z) + \ldots \tag{8}$$

where Y is the Bessel function of the second kind. The first series converges for any combination of ρ and z while the second converges only for $\rho>z$. Finally, the scattering function k_b in Eqs. (1) and (3) for the anomalous diffraction case is:

$$k_b(\alpha,\theta) = A^2(\alpha\theta)/(\alpha^{b-2}) \tag{9}$$

where $A^2 = (\mathrm{Im}A)^2 + (\mathrm{Re}A)^2$ as expressed by Eqs. (6-8). To quantify the error of the Fraunhofer diffraction approximation when anomalous diffraction conditions are present we have generated near forward scattering signatures based on anomalous diffraction theory for NBS standard reference material (SRM) 1003a.

RESULTS

A plot of the intensity normalized over the angle range 0-2.7° is shown in Fig. 1 for NBS 1003a, which contains particle sizes ranging from 5-63μm. As expected when the value of the refractive indices approach unity, the intensity at larger angles increases as the refracted light interferes with the diffracted light in this angle range. When the ratio of the refractive indices is greater than 1.2 the anomalous diffraction results agree with Fraunhofer diffraction. It should also be noted that the anomalous diffraction results in this angle range were verified by Lorenz-Mie theory.

Figure 2 is a plot of the relative detector output vs. detector number for the RSI ring detector. Results are found by integrating the intensity distribution of Fig. 1 over each detector area. Refractive indices close to one show more energy on the outer rings. Again, recall that results are for the same particle size distribution, the only variable is the refractive index.

If an instrument scattering matrix K is calculated using a Fraunhofer diffraction kernel k_b then sizing errors will result if the actual scattering process is not accurately modeled by diffraction theory. The varying scattering signatures of Fig. 2 represent different I vectors in Eq. (2), which for the same K must give different measured size distributions represented by N. Since small particles scatter light at relatively large angles, the anomalous diffraction (refractive scatter) contributions on the outer detectors for small refractive indices in Fig. 2 appear to come from small particles to an instrument based on Fraunhofer theory. This can be seen from the reconstructed size distributions shown in Fig. 3 where a small particle mode (in the lower size classes) appears for the two lowest refractive indices. These resulting errors are quantified in terms of representative size parameters as would be measured by an instrument based on Fraunhofer diffraction (D_{V_x} is defined according to ASTM E799 such that the volume fraction of particles with diameters smaller than D_{V_x} is x, and $\alpha_{V_x} = \pi/\lambda D_{V_x}$).

The data of Fig. 4 show three regimes, two for the limiting cases of very small and very large relative refractive indices and a third in the intermediate m range. For very large refractive indices, the refracted light is scattered into large angles beyond the collection aperture of the system (see Fig. 1). Here the Fraunhofer diffraction theory is applicable, and the errors are small. For very small refractive indices, the scattering is very small because the contrast between the particle and the medium is very weak. Here, although the refracted light does mix with the near-forward diffracted light the refracted contribution is weak and again diffraction theory is reasonable good as demonstrated by small errors. In the intermediate refractive index range (from about 1.004 to 1.2 in this example), the refracted light contribution is significant and falls into the collection aperture. This causes a dip in the curves of Fig. 4, i.e. the refracted light entering the near-forward angles cause the instrument based on diffraction theory to undersize by as much as 70%. In summary, significant errors in particle size distribution reconstructions based on Fraunhofer diffraction theory will occur when the ratio of the refractive indices is in an intermediate range. Better approximations or the full Lorenz-Mie scattering theory should be used in instruments operating in these refractive index ranges.

ACKNOWLEDGMENTS

This research was supported by the Air Force Office of Science Research, Air Force Systems Command, USAF, under grant AFOSR-84-0187, Dr. Julian Tishkoff, program manager. The U.S. government is authorized to reproduce and distribute reprints for governmental purposes notwithstanding any copyright notation thereon.

REFERENCES

H. C. van de Hulst, *Light Scattering by Small Particles*, John Wiley and Sons, New York (1957).

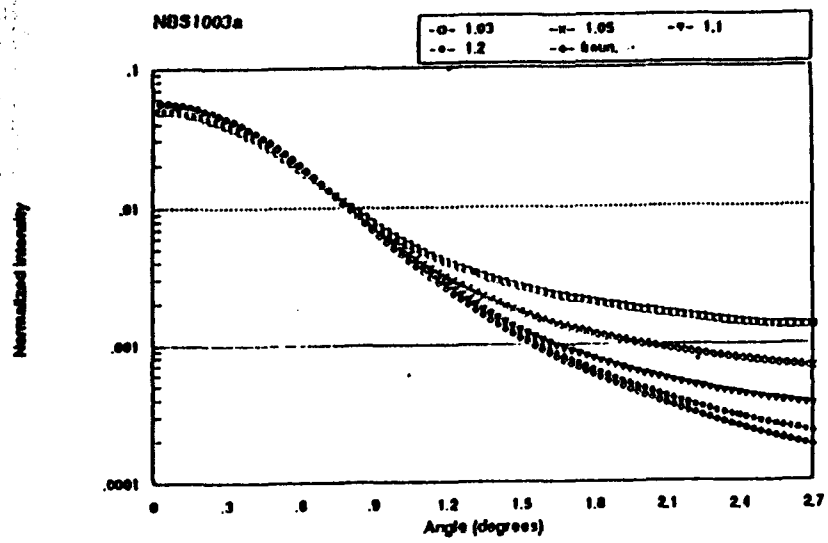

Figure 1. Forward scattering signature of SRM NBS1003a particle size distribution based on Fraunhofer and anomalous diffraction theory (for this particle size distribution, and angle range anomalous diffraction and Mie theory gave equal results). Refractive indices of particles relative to medium of 1.025, 1.05, 1.1, and 1.2 are used in anomalous diffraction calculations.

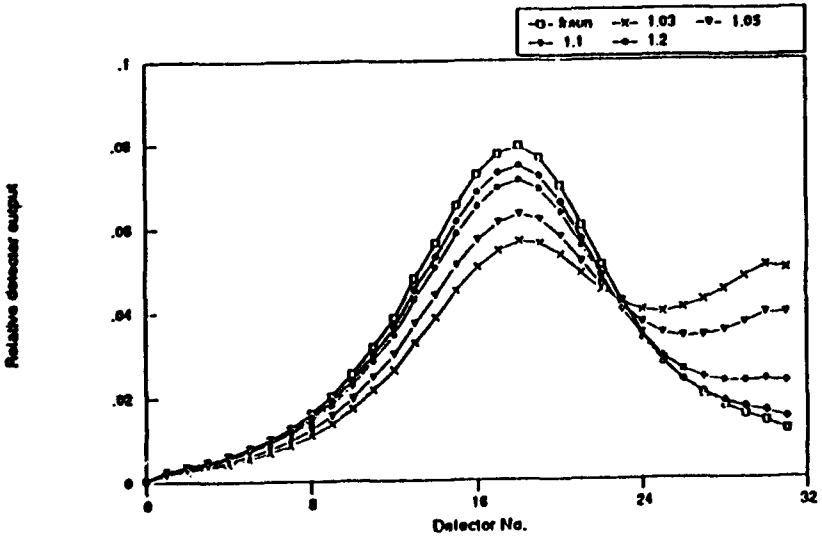

Figure 2. Forward scattering signatures as indicated by relative detector outputs of an annular ring detector geometry. The data were calculated based on Fraunhofer and Anomalous diffraction theories. Refractive indices of particles relative to medium are 1.03, 1.05, 1.1, and 1.2 for the Anomalous

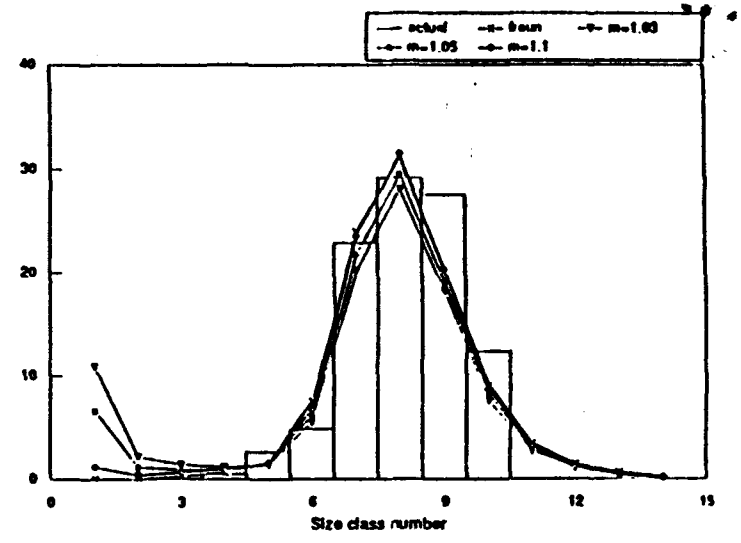

Figure 3. Percent volume in size class vs. size class. Particle size distribution is distributed over 15 size classes corresponding to a Malvern commercial instrument. Values are calculated by inverting the results of figure 2.

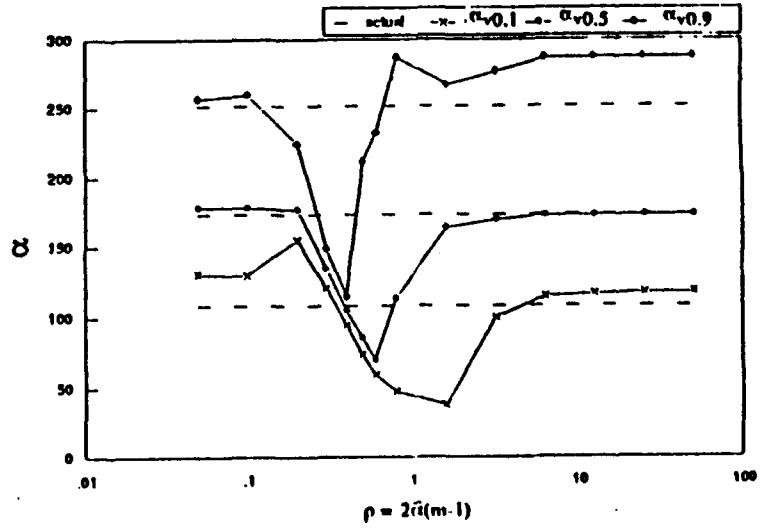

Figure 4. Plot of $\alpha_{v0.1}$, $\alpha_{v0.5}$, and $\alpha_{v0.9}$ vs. phase lag ρ. Calculated values are found from inverting the anomalous diffraction predicted scattering pattern assuming Fraunhofer diffraction.